Tel-Aviv University

Faculty of Engineering

School of Electrical Engineering

אוניברסיטת תל-אביב

הפקולטה להנדסה

בי"ס להנדסת חשמל

High order Laser beam modes

Project identifier: 14-2-1-839

Final Report

Author:

038022869 Guy Shtief (Sztajf) גיא שטייף

Instructor: מנחה:

Tel Aviv University Shoam Shwartz שוהם שוורץ

The study took place at:

a) The laboratory of Prof. Shlomo Ruschin, Tel-Aviv University.

b) The laboratory of Dr. Michael Golub, Tel-Aviv University.

Table 1: Table of contents

Chapter 1: Overview

This study consists of simulation methods and a computerized design of an optical system, with an emphasis on designing a multi-channel optical matched filter.

The study will explore the multi-mode optical system portrayed abstractly by the block diagram in, and more specifically, the realization of that system portrayed in Figure 0–2[1].

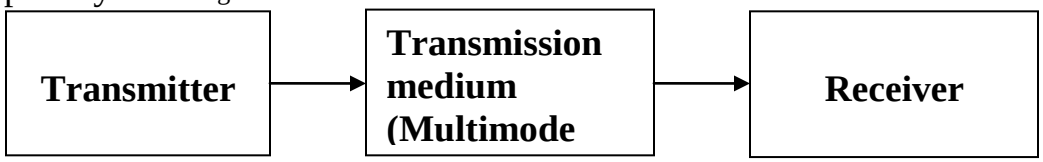

Figure 0–1: A block diagram of an optical communication system

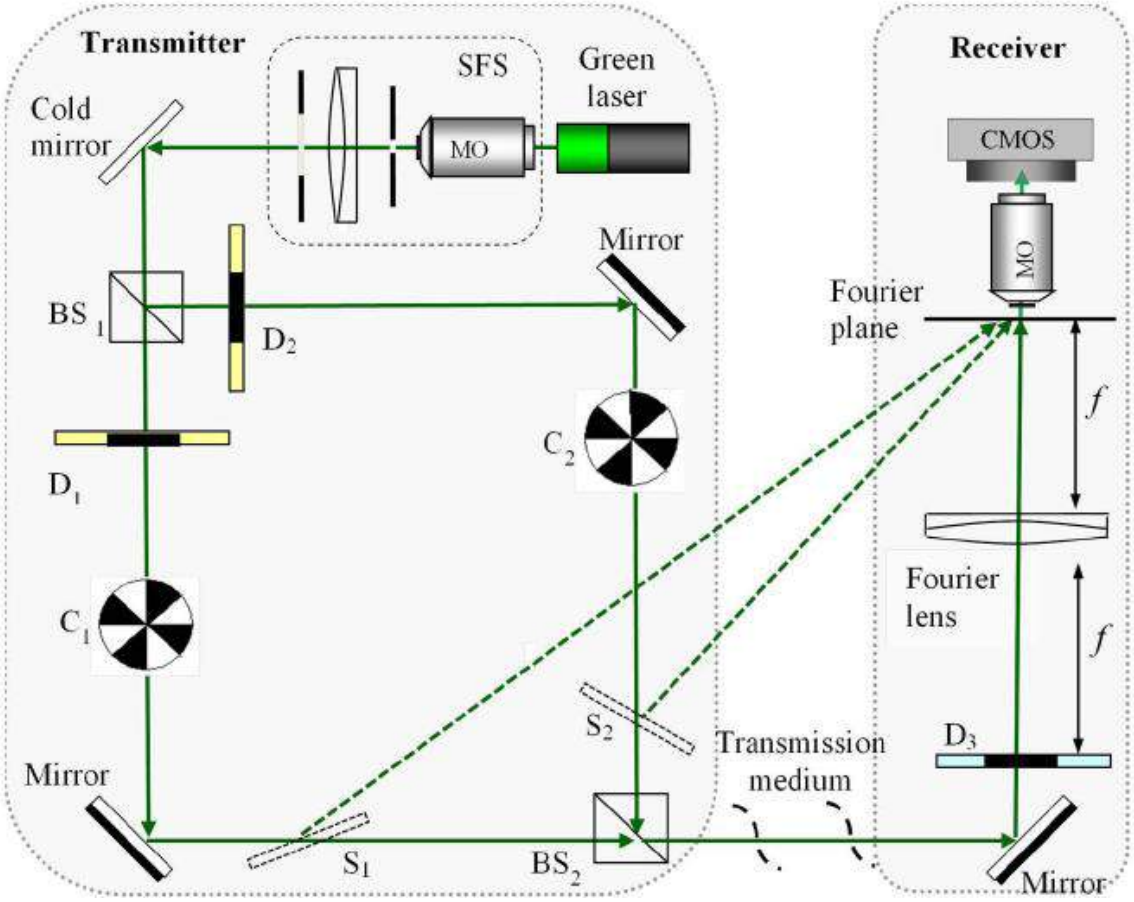

Figure 0–2 (Color online) Experimental optical setup for MM free-space optical communication system. SFS: spatial filter system; BS1 and BS2: beam splitters; S1 and S2: beam samplers; D1, D2, D3: DOEs; C1 and C2: choppers; MO: micro objective; CMOS:CMOS camera

[1] Will be discussed in detail in Chapter 2: Foreword

Chapter 2: Foreword

Study goals

The goals of this study are the following:

1) Establish a robust MATLAB algorithm code which allows simulations of optical wave propagations within an optical system.
2) Using said simulations to verify the validity of a multi-mode optical matched filter that was planned theoretically and compare those simulations to those obtained by another study[1] in a laboratory.

Study motivation: Multiplexing multi-mode optical communication

Nowadays, the optical communication field dominates the long-distance information transferring networks, such as the internet, telephones etc.
As time went by, the information transfer rate increased as it's price dropped (for example: The internet), however, this increasing rate is approaching an upper boundary[i][ii], which causes a bottleneck phenomenon in **single**-mode optical fibers (The current technology is approaching a theoretical boundary of 100Tb/s[iii]).

The approach to overcome the information rate boundary

Strenuous efforts are made and invested both in the industry as in the academy to remedy that boundary, and one of the optimal solutions is the realization of **multi**-mode optical fibers (as opposed to the, commonly used, single-mode ones).

Analogy between this study and another

This study was initiated to provide a tool of validation to support the study conducted by P.hd candidate Shoam Swartz, as the latter was conducted almost exclusively based on theoretical design and lab experimentation, while the former is a theoretical/physical simulation of the physics involved

[1] Shoams Study

Chapter 3: Theoretical Background

In this chapter we would like to reintroduce two popular concepts of optics and communication systems, those are Fourier optics and Bessel functions.

Chapter 3.1 Fourier optics

The wave equation is the mathematical basis for all the phenomena of a wave.

It can be obtained by Maxwell's Equations (Eq.1-4) as follows:

1 $\nabla \times \vec{\mathbf{E}} = -\frac{\partial \vec{\mathbf{B}}}{\partial t}$ ($\vec{\mathbf{E}}$ is an electric field, $\vec{\mathbf{B}}$ is a magnetic influx density,

∇ is the vector operator of $\left(\frac{\partial}{\partial x}, \frac{\partial}{\partial y}, \frac{\partial}{\partial z}\right)$)

2 $\nabla \times \vec{\mathbf{H}} = \vec{\mathbf{J}} + \frac{\partial \vec{\mathbf{D}}}{\partial t}$ ($\vec{\mathbf{H}}$ is a magnetic field, $\vec{\mathbf{J}}$ is a current density,

$\vec{\mathbf{D}}$ is an electric influx density)

3 $\nabla \cdot \vec{\mathbf{D}} = \rho$ **;** $\vec{\mathbf{D}} \overset{\text{in linear isotropic media}}{=} \varepsilon \vec{\mathbf{E}}$ (ρ is the spatial electric charge density,

ε is the dielectric coefficient of the media)

4 $\nabla \cdot \vec{\mathbf{B}} = 0$ **;** $\vec{\mathbf{B}} \overset{\text{in linear isotropic media}}{=} \mu \vec{\mathbf{H}}$ (μ is the permeability coefficient of the media)

Solving those equations for homogeneous media that lacks charges and currents, and applying the Lagrange vector identity of $\nabla \times \nabla \equiv -\nabla^2$, yields the wave equation (eq.5),

5 $\nabla^2 \vec{\mathbf{E}} = \frac{1}{c^2} \frac{\partial^2}{\partial t^2} \vec{\mathbf{E}}$

Where $c = 3 \times 10^8 [m/s]$ is the speed of light in free space, ∇^2 is the Laplace operator, and *t* stands for time in seconds (or nano-seconds).

Limiting the discussion to fields of the mathematical form of:
$U(\mathbf{r},t)=a(\mathbf{r})\exp\left(j\varphi(\mathbf{r})\right)\exp\left(j2\pi\nu t\right)$,
the wave equation, then, degenerates into Helmholtz equation (Eq.6

$\nabla^2\vec{\mathbf{E}}+k^2\vec{\mathbf{E}}=0$ **(k is the wave number and it satisfies** $k=\frac{\omega}{c}=2\pi\frac{\nu}{c}=2\pi\frac{1}{\lambda}$**)**6).

6 $\nabla^2\vec{\mathbf{E}}+k^2\vec{\mathbf{E}}=0$ (k is the wave number and it satisfies $k=\frac{\omega}{c}=2\pi\frac{\nu}{c}=2\pi\frac{1}{\lambda}$)

Now, given some abstract distribution of an electro-magnetic field at plane z=0, $u(x,y;0)$, it can be shown[1], using the Helmholtz equation (Eq.6) , that the distribution at plane z=z', $u(x,y;z')$ must satisfy,

7 $$u(x,y;z)=\int_{-\infty}^{\infty}\int_{-\infty}^{\infty}\left[\begin{array}{l}A\left(\frac{\alpha}{\lambda},\frac{\beta}{\lambda};0\right)\exp\left[j\frac{2\pi}{\lambda}\left(\sqrt{1-\alpha^2-\beta^2}\right)z\right]\times\\ \exp\left[j2\pi\left(\frac{\alpha}{\lambda}x+\frac{\beta}{\lambda}y\right)\right]d\left(\frac{\alpha}{\lambda}\right)d\left(\frac{\beta}{\lambda}\right)\end{array}\right]$$

whereas,

8 $$u(x,y;0)=\int_{-\infty}^{\infty}\int_{-\infty}^{\infty}A\left(\frac{\alpha}{\lambda},\frac{\beta}{\lambda};0\right)\exp\left[j2\pi\left(\frac{\alpha}{\lambda}x+\frac{\beta}{\lambda}y\right)\right]d\left(\frac{\alpha}{\lambda}\right)d\left(\frac{\beta}{\lambda}\right)$$

where, $\alpha=\sin\theta_x=\frac{k_x}{k},\beta=\sin\theta_y=\frac{k_y}{k}$; $\nu_x=\frac{\alpha}{\lambda},\nu_y=\frac{\beta}{\lambda}$,

and, $A(\nu_x,\nu_y;0)$ is referred to as, the *Angular Spectrum* of $u(x,y;0)$,

9 $$A\left(\frac{\alpha}{\lambda},\frac{\beta}{\lambda};0\right)=\int_{-\infty}^{\infty}\int_{-\infty}^{\infty}u(x,y;0)\exp\left[-j2\pi\left(\frac{\alpha}{\lambda}x+\frac{\beta}{\lambda}y\right)\right]dxdy$$

Alternatively:

10 $$u(x,y;z)=\Im\left\{\underbrace{A\left(\frac{\alpha}{\lambda},\frac{\beta}{\lambda}\right)}_{\text{Angular Spectrum of }u(x,y;0)}\cdot\underbrace{\exp\left[j\frac{2\pi}{\lambda}\left(\sqrt{1-\alpha^2-\beta^2}\right)z\right]}_{H\left(\frac{\alpha}{\lambda},\frac{\beta}{\lambda};z\right)\text{ transfer function of free space}}\right\}$$

where $\Im$ in Eq.10 is the 2 dimensional *Fourier Transform* such that for any 2-dimensional function, *g*, it's Fourier transform is given by *G*

---

[1] $\gamma=\sqrt{1-\alpha^2-\beta^2}$

11 $G(x,y)=\Im\{g(\xi,\eta)\}\triangleq\int_{-\infty}^{\infty}\int_{-\infty}^{\infty}g(\xi,\eta)\exp\left(-2\pi j(\xi x+\eta y)\right)d\xi d\eta$

Utilizing the *convolution theorem*[1] for Continuous Fourier Transform,

12 $u(x,y;z)=u(x,y;0)*\Im\left\{\exp\left[j\frac{2\pi}{\lambda}\left(\sqrt{1-\alpha^2-\beta^2}\right)z\right]\right\}$

The denotation of '*', is the 2 dimensional convolution operator, which is to be taken as following,

13 $u*w\triangleq\int_{-\infty}^{\infty}u(\xi,\eta)w(x-\xi,y-\eta)d\xi d\eta$

At the form of Eq.7, it is said that u satisfies the *Rayleigh-Sommerfeld* propagation.

Even though Eq.7 provides a closed formula to evaluate wave propagations, it is still challenging to evaluate it, both analytically, and numerically, therefore we will rely on approximations to it such as *Fresnel-Kirchhoff*, AKA the *Paraxial approximation* for wave propagation.

Given the angles of the wave propagation (relative to the optical axis) are small, we may use the first terms of Taylor expansion for $\sqrt{1-\alpha^2-\beta^2}$, such that,

14 $\sqrt{1-\alpha^2-\beta^2}=\sqrt{1-(\lambda\nu_x)^2-(\lambda\nu_y)^2}\cong 1-0.5(\lambda\nu_x)^2-0.5(\lambda\nu_y)^2$

using this *paraxial approximation*, *H*, simplifies into,

15 $H(\nu_x,\nu_y)=\exp\left[j\frac{2\pi}{\lambda}\left(\sqrt{1-\alpha^2-\beta^2}\right)z\right]\sim\exp(jkz)\exp\left[j\pi\lambda z\left(\nu_x^2+\nu_y^2\right)\right]$

which, in the *xy* plane, has the form of,

16 $h(x,y)=\Im^{-1}\left\{H(\nu_x,\nu_y)\right\}=\frac{\exp(jkz)}{j\lambda z}\exp\left[j\frac{\pi}{\lambda z}\left(x^2+y^2\right)\right]$

($\Im^{-1}$ is the inverse Fourier Transform[2])

17 $u(x,y;z)=u(x,y;0)*\left[\frac{\exp(jkz)}{j\lambda z}\exp\left[j\pi\lambda z\left(\nu_x^2+\nu_y^2\right)\right]\right]=u(x,y;0)*h(x,y;z)$

or, much more compactly:

---

[1] $\Im\{f\cdot g\}=F*G$

[2] $\Im^{-1}\{H(\xi,\eta)\}\triangleq\int_{-\infty}^{\infty}\int_{-\infty}^{\infty}H(\xi,\eta)\exp\left(+2\pi j(\xi x+\eta y)\right)d\xi d\eta$

18 $$u(x,y;z)=\left[\begin{array}{l}\frac{j}{\lambda z}\exp\left(-j\frac{2\pi z}{\lambda}\right)\exp\left[j\frac{\pi}{z\lambda}\left(x^2+y^2\right)\right]\times \\ \int_{-\infty}^{\infty}\int_{-\infty}^{\infty}u(\xi,\eta;0)\exp\left[j\frac{\pi}{\lambda z}\left(\xi^2+\eta^2\right)\right]\exp\left[-j\frac{2\pi}{\lambda z}\left(x\xi+y\eta\right)\right]d\xi d\eta\end{array}\right]$$

or, ultimately, in the form that will be carried out in the simulations, and will be referenced many times more, throughout this paper:

19 $$u(x,y;z)=\left[\begin{array}{l}\frac{j}{\lambda z}\exp\left(-j\frac{2\pi z}{\lambda}\right)\exp\left[j\frac{\pi}{z\lambda}\left(x^2+y^2\right)\right]\times \\ \Im\left\{\left(\lambda z\right)^2 u_{in}\left(\lambda z\xi,\lambda z\eta;0^+\right)\exp\left[j\pi\lambda z\left(\xi^2+\eta^2\right)\right]\right\}\end{array}\right]$$

This final form is very conducive to our simulations cause, as we will show in later chapters.

Another approximation, which we will use, is the *Fraunhofer Far Field* approximation, which is fairly accurate as $z\to\infty$ (even though in our set of parameters, $z\sim 4[m]$ is pretty much enough), and also, $z\gg\max\left\{\frac{k}{2}\left(\xi^2+\eta^2\right)\right\}$

This approximation would simplify Eq.19 into,

20 $$u(x,y;z)=\frac{j}{\lambda z}\exp\left(-j\frac{2\pi z}{\lambda}\right)\exp\left[j\frac{\pi}{z\lambda}\left(x^2+y^2\right)\right]\cdot\Im\left\{\left(\lambda z\right)^2 u_{in}\left(\lambda z\xi,\lambda z\eta;0^+\right)\right\}$$

Notice that Eq.20 gives the Fourier Transform of the input wave, multiplied by a z dependent phase, and a parabolic phase.
In fact Eq.20 implies that in order to get the Fourier Transform of an optical signal, it should be allowed to propagate to some "long" distance, and measured by intensity (which will ignore the parabolic and constant phases).

Chapter 3.2 Laguerre-Gaussian beams

The *Generalized Laguerre polynomials*[1][iv] are denoted $L_n^{(\alpha)}(x)$ and they satisfy the ODE (Ordinary Differential Equation) of,

21 $xy"+(\alpha+1-x)y'+ny=0$

which has few forms of solutions, one of them being:

22 $L_n^{(\alpha)}(x)=\sum_{i=0}^{n}(-1)^i\binom{n+\alpha}{n-i}\frac{x^i}{i!}$

The first four Laguerre polynomials, $\left\{L_n^{\alpha}(x)\right\}_{n=0}^{3}$,are presented in Table 2.

Table 2: The first four Laguerre polynomials

n	$L_n^{\alpha}(x)$
0	1
1	$-x+\alpha+1$
2	$\frac{x^2}{2}-(\alpha+2)x+\frac{(\alpha+2)(\alpha+1)}{2}$
3	$-\frac{x^3}{6}+\frac{(\alpha+3)x^2}{2}-\frac{(\alpha+2)(\alpha+3)x}{2}+\frac{(\alpha+1)(\alpha+2)(\alpha+3)}{6}$

Our interest in those polynomials arises from the solution of the paraxial wave equation (which was obtained using) given a cylindrically symmetric problem.

In a cylindrically symmetric problem, Eq.19 gives a solution in the form of,

23 $u_{\ell p}(r,\phi,z)=\left[\begin{array}{l} C_{\ell p}^{LG}\frac{w_0}{w(z)}\left(\frac{r\sqrt{2}}{w(z)}\right)^{|\ell|}\exp\left(-\frac{r^2}{w^2(z)}\right)L_p^{|\ell|}\left(\frac{2r^2}{w^2(z)}\right)\cdot \\ \exp\left(-jk\frac{r^2}{2R(z)}\right)\exp(j\ell\phi)\exp\left[j(2p+|\ell|+1)\zeta(z)\right]\end{array}\right]$

where, (r,ϕ,z), are the cylindrical coordinates (sometimes denoted (ρ,φ,z)).

$C_{\ell p}^{LG}$ is chosen such that,

24 $\int_0^{\infty}\int_0^{2\pi}\left|u_{\ell p}(r,\phi,0)\right|^2 rdrd\phi=1$

as a power normalization constant, which yields,

[1] Also, the *Associated Laguerre polynomials*

25 $C_{\ell p}^{LG} = \frac{1}{w_0}\sqrt{\frac{2p!}{\pi\left(p+|\ell|\right)!}}$

the rest of the parameters are explicitly explained in Table 3.Table 3: Laguerre Gauss Parameters

Table 3: Laguerre Gauss Parameters

Parameter	Formula	Name and Meaning
z	-	Distance from input plane of the beam.
z_0	$z_0 = \pi w_0^2 / \lambda$	Reyleigh's distance – The distance at which the waveform waist is $w(z_0) = \sqrt{2}w_0$ (see (1.1f))
k	$k = 2\pi / \lambda$	Beam's wave number whereas λ is it's wavelength.
w_0	$w_0 = \sqrt{z_0 \lambda / \pi}$	Beam waist, which is, the *second moment* of $u \cdot u^*$.
$w(z)$	$w(z) = w_0\sqrt{1+\left(\frac{z}{z_0}\right)^2}$	Beam waist, as the beam propagates as function of *z*.
$R(z)$	$R(z) = z\left[1+\left(\frac{z_0}{z}\right)^2\right]$	Curvature radius of the beam front, contributes a spherical phase to the beam.
$\zeta(z)$	$\zeta(z) = \arctan\left(\frac{z}{z_0}\right)$	Guoy phase. Contributes a *z* dependant phase to the beam.
E_0	$E_0 = \left\|E(0,0)\right\|$	Field's amplitude at input plane.

Also, when applying $\ell = p = 0$, and $z = 0$, Eq.23 is referred to as: a *Gaussian wave* (introduced in Eq.26),

26 $u(x,y;0) = E_0 \exp\left(-\frac{x^2+y^2}{w_0^2}\right)$

it is the most fundamental wave in the field of optics, and when discussing other waveforms, most analogies are made in comparison to it.

Also, when allowing Eq.26 to propagate, using Eq.19, we obtain the *z* dependant Gaussian wave, portrayed as follows,

27 $u(x,y;z) = E_0 \frac{w_0}{w(z)}\exp\left(-\frac{x^2+y^2}{w^2(z)}\right)\exp\left(-jk\frac{x^2+y^2}{2R(z)} - jkz + j\zeta(z)\right)$

A note about *Eigen-Fucntions* to the wave equation

It is important to note that while Eq.27 are solutions (plural for all $\ell, p \in \square$) to Eq.19, their magnitude, $\left|u_{\ell p}(r,\phi,z)\right|$ is an *eigen-function* of 3.19, that is, $\left|u_{\ell p}(r,\phi,z_2)\right|$ differs from $\left|u_{\ell p}(r,\phi,z_1)\right|$ only by a multiplication constant, and scaling by the distance $z_2 - z_1$ (in respect to *x* and *y* [or *r* and ϕ]), meaning that $\left|u_{\ell p}(r,\phi,z_2)\right|$ has the same functional pattern as $\left|u_{\ell p}(r,\phi,z_1)\right|$, or,

$$\left|u_{\ell p}(r,\phi,z_2)\right| = c_1\left|u_{\ell p}(c_2 r, c_3\phi, z_1)\right|$$

where $\{c_i\}_{i=1}^{3}$ aren't dependant on the coordinates, r,ϕ,x,y , but only on z_2, z_1

Let's take for example, a Gaussian wave (Eq.26) which is traveling from $z=0$ to $z=z_p$, it must satisfy Eq.19 and it's magnitude is given by:

$$\left|u(x,y;z)\right| = \frac{\lambda z w_0^2}{\pi}\left|\Im_{2d}\left\{\exp\left(-\frac{(\lambda z\xi)^2+(\lambda z\eta)^2}{w_0^2}\right)\exp\left[j\pi\lambda z\left(\xi^2+\eta^2\right)\right]\right\}\right|$$

evaluating the 2-dimensional Fourier transform's magnitude we obtain:

$$\left|u(x,y;z)\right| = \frac{w_0^2}{\pi}\frac{w_0}{w(z)}\exp\left(-\frac{x^2+y^2}{w^2(z)}\right)$$

it is obvious that both the last two equations bear the same functional pattern as explained using handwaving in last paragraph.

Chapter 3.3 Jacobi-Anger Expansion and Bessel functions

Bessel Functions are, in mathematical respect, the canonical solutions $y(x)$ of the Bessel's ODE of,

28 $x^2 \frac{d^2y}{dx^2} + x\frac{dy}{dx} + \left(x^2 - \alpha^2\right)y = 0 \ \ (\alpha \in \square)$

The *Bessel functions of first kind* are denoted $J_\alpha(x)$, and are plotted in Figure 3.

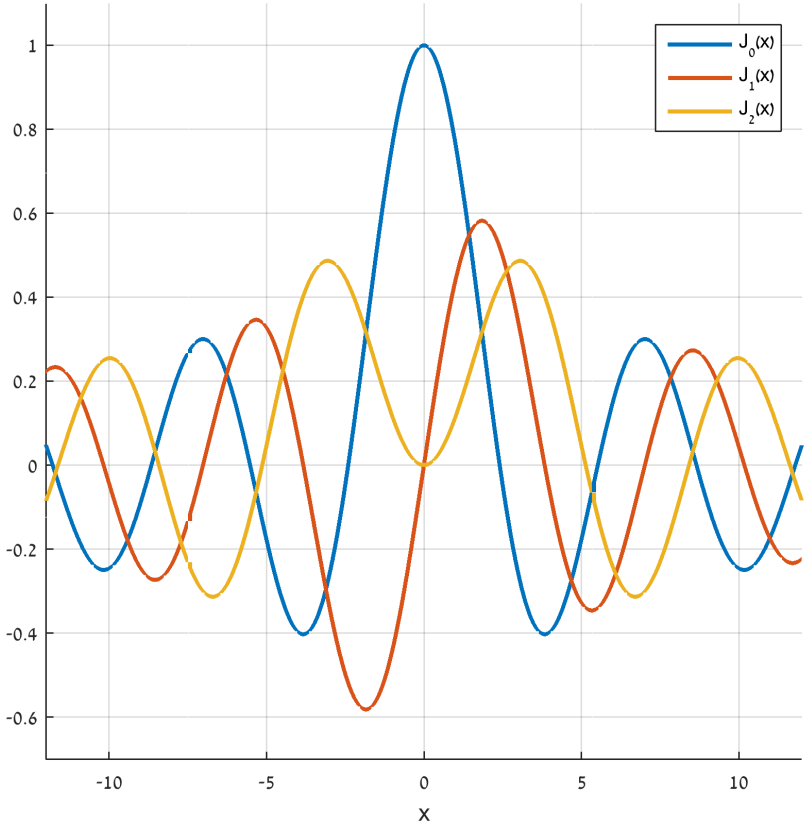

Figure 3: Plot of Bessel function of the first kind, $J_\alpha(x)$, for integer orders α = 0, 1, 2

Code simulated:
`One_Dimensional_Bessel_functins_plot.m`

The Jacobi-Anger expansion is given by [v][vi],

29 $\exp\left(jz\sin\theta\right)=\sum_{n=-\infty}^{\infty}J_n\left(z\right)\exp\left(jn\theta\right)$**,**

Substituting, $z=\delta r$ $\left(r^2=x^2+y^2\right)$ and $\theta=2\pi\nu_x x-\phi$ $\left(\phi=\arctan 2\left(y/x\right)\right)$, into Eq.29, we obtain (δ and ν_x will be explained and verified in Chapter 4 using simulations):

30 $\exp\left(j\delta r\sin\left(2\pi\nu_x x-\phi\right)\right)=\sum_{n=-\infty}^{\infty}J_n(\delta r)\exp\left(-jn\phi\right)\exp\left(jn2\pi\nu_x x\right)$

Multiplying Eq.30 by Eq.26 (a Gaussian-Beam), we obtain,

31 $\exp\left(j\delta r\sin\left(2\pi\nu_x x-\phi\right)-\frac{r^2}{w_0^2}\right)=\sum_{n=-\infty}^{\infty}J_n(\delta r)\exp\left(-jn\phi\right)\exp\left(-\frac{r^2}{w_0^2}\right)\exp\left(jn2\pi\nu_x x\right)$

or, in the denotation of Eq.23 (The Laguerre-Gauss modes),

32 $u_{00}\left(r\right)\exp\left(j\delta r\sin\left(2\pi\nu_x x-\phi\right)\right)=\sum_{n=-\infty}^{\infty}u_{00}\left(r\right)J_n(\delta r)\exp\left(-jn\phi\right)\exp\left(jn2\pi\nu_x x\right)$

Assessing the pattern of Eq.32, it is amazing to perceive, that transmitting a Gaussian beam through a *Phase Mask*, in the form of Eq.32 left hand side, results in a generalized superposition of Bessel-Gaussian waveforms with angular and linear phase with a radial form of a Bessel function.

In the next topic of *Bessel-Gauss* beams, we will apply this trait, and with further conclusions, we will be able to make predictions of the far field, or the Fourier transform of Eq.32.

A note about Phase Modulation

A reader, well educated in the area of *Communication Systems*, will notice that the left hand side of Eq.30 is in the mathematical form of a *Phase Modulation* applied to a carrier signal, it is a popular method to transmit information from a *Transmitter*, through a *Channel* (with noise), towards a *Receiver*.

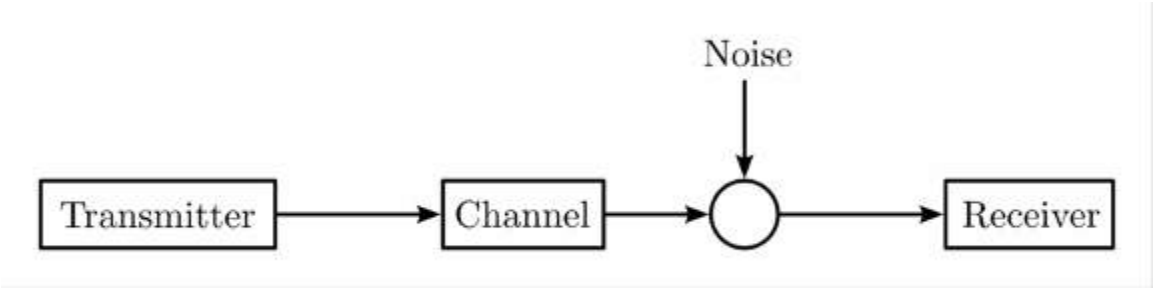

Figure 4: A block diagram model for transmitting information through a noisy channel

It does so, in encoding information, as variations in the instantaneous phase of the carrier wave, doing so, it obtains lower *SNR* (signal to noise ratio), and allows better transmitting properties.

Phase Modulation, in general, is widely used for transmitting radio waves and is an integral part of many digital transmission coding schemes that underlie a wide range of technologies like WiFi, GSM, and satellite television.
It essentially changes the phase angle of the complex envelope in direct proportion to the message signal.

Chapter 3.4 Bessel Functions and Bessel-Gaussian beams

It can be shown that the Bessel functions of first kind (Eq.28) can be expressed as a generalized superposition of generalized Laguerre polynomials for some arbitrarily parameter t[vii],

33 $$\frac{J_\alpha(x)}{\left(\frac{x}{2}\right)^\alpha}=\frac{e^{-t}}{\Gamma(\alpha+1)}\sum_{k=0}^{\infty}\frac{L_k^{(\alpha)}\left(\frac{x^2}{4t}\right)}{\binom{k+\alpha}{k}}\frac{t^k}{k!}$$

where Γ denotes the *Gamma Function*.
Substituting $\alpha=\ell\left(\in\mathbb{N}\right)$, $x=2\sqrt{2\kappa\zeta}$, $k=p$, $t=\zeta$, whereas $\kappa=r^2/w_0^2$ and $\zeta=\exp\left(j2\pi\nu_y y\right)$, (and discarding these variables, as we would like to reuse x) we obtain,

34 $$\frac{J_\ell\left(2\sqrt{2\kappa\zeta}\right)}{\left(\frac{2\sqrt{2\kappa\zeta}}{2}\right)^\ell}=\frac{e^{-\zeta}}{\Gamma(\ell+1)}\sum_{p=0}^{\infty}\frac{L_p^\ell\left(\frac{\left(2\sqrt{2\kappa\zeta}\right)^2}{4\zeta}\right)}{\binom{p+\ell}{p}}\frac{\zeta^p}{p!}$$

(the new parameters role in our study will be clarified in Chapter 4)

Reorganizing Eq.34 it then yields:

35 $$\exp(\zeta)J_\ell\left(2\sqrt{2\kappa\zeta}\right)=\frac{1}{\Gamma(\ell+1)}\sum_{p=0}^{\infty}\frac{\ell!}{(p+\ell)!}2^{\ell/2}\kappa^{\ell/2}L_p^\ell(2\kappa)\zeta^{p+\ell/2}$$

Substituting $\Gamma(\ell+1)=\ell!$ (assuming $\ell\in\mathbb{N}$) yields even further:

36 $$\exp(\zeta)J_\ell\left(2\sqrt{2\kappa\zeta}\right)=\sum_{p=0}^{\infty}\frac{1}{(p+\ell)!}2^{\ell/2}\kappa^{\ell/2}L_p^\ell(2\kappa)\zeta^{p+\ell/2}$$

multiplying both sides by the term $\exp\left(j\ell\left(2\pi\nu_x x+\phi\right)\right)$ (not to be confused with the x that was discarded from Eq.33) yields

$$\exp(\zeta)J_\ell\left(2\sqrt{2\kappa\zeta}\right)\exp\left(j\ell\left(2\pi\nu_x x+\phi\right)\right)=\ldots$$

37
$$\ldots\sum_{p=0}^{\infty}\exp\left(j\ell\left(2\pi\nu_x x+\phi\right)\right)\frac{2^{\ell/2}\kappa^{\ell/2}L_p^\ell(2\kappa)\zeta^{p+\ell/2}}{(p+\ell)!}$$

the LHS (left hand side) of Eq.37, multiplied by $\exp(-\kappa)$, is called a Bessel-Gauss beam, it is a paramount waveform in this study, since, as we will discuss in later chapters, has a significant role in optical communications.

for clarification purposes, we will present the Left Hand Side LHS (left hand side) of Eq.37 in the proper terms,

$$\mathbf{38}\quad u_{\ell}^{BG}(r,\phi;0)=\exp\left(-\frac{r^2}{w_0^2}\right)\exp\left(j2\pi\nu_y y\right)J_{\ell}\left(\frac{2\sqrt{2}r}{w_0}\exp\left(j\pi\nu_y y\right)\right)\exp\left(j\ell\left(2\pi\nu_x x+\phi\right)\right)$$

where $r=\sqrt{x^2+y^2}$, $x=r\cos\phi$, $y=r\sin\phi$.

Also, (ν_x,ν_y) are the displacements of Eq.37 *Angular Spectrum* in the *Spatial Frequency* plane, and they will be discussed again later on.

For completeness, and to support the last subchapter regarding the Jacobi-Anger expansion, we shall present Eq.37 (with the Gaussian addition) in terms of Laguerre-Gauss superposition,

$$\mathbf{39}\quad \begin{aligned}&\exp\left(-\frac{r^2}{w_0^2}\right)\exp\left(j2\pi\nu_y y\right)J_{\ell}\left(\frac{2\sqrt{2}r}{w_0}\exp\left(j\pi\nu_y y\right)\right)\exp\left(j\ell\left(2\pi\nu_x x+\phi\right)\right)=\ldots\\&\ldots\sum_{p=0}^{\infty}\exp\left(j\ell\left(2\pi\nu_x x\right)\right)\exp\left(j\left(p+\ell/2\right)2\pi\nu_y y\right)\sqrt{\frac{w_0^2\pi}{2p!(p+\ell)!}}u_{\ell p}^{LG}(r,\phi;0)\end{aligned}$$

and we can now conclude that, for $\nu_x=\nu_y\equiv 0$,

$$\mathbf{40}\quad u_{\ell}^{BG}(r,\phi;0)\Big|_{\nu_x=\nu_y\equiv 0}=\exp\left(-\frac{r^2}{w_0^2}\right)J_{\ell}\left(\frac{2\sqrt{2}r}{w_0}\right)\exp\left(j\ell\phi\right)=\sum_{p=0}^{\infty}\sqrt{\frac{w_0^2\pi}{2p!(p+\ell)!}}u_{\ell p}^{LG}(r,\phi;0)$$

A notable conclusion of equations 39-40 is that a Bessel-Gauss beam mode is in fact a superposition of ($\ell=const$) Laguerre-Gauss beam modes with only the *p* index varying, this conclusion, also sheds some light on the waveforms discussed in the Jacobi-Anger subchapter, earlier.

Continuing from Eq.37, we take an infinite sum on both sides over $\ell\in\mathbb{Z}$,

$$\mathbf{41}\quad \begin{aligned}&\exp(\zeta)\sum_{\ell=-\infty}^{\infty}J_{\ell}\left(2\sqrt{2\kappa\zeta}\right)\exp\left(j\ell\left(2\pi\nu_x x+\phi\right)\right)=\ldots\\&\ldots\sum_{\ell=-\infty}^{\infty}\sum_{p=0}^{\infty}\exp\left(j\ell\left(2\pi\nu_x x+\phi\right)\right)\frac{2^{\ell/2}\kappa^{\ell/2}L_p^{\ell}\left(2\kappa\right)\zeta^{p+\ell/2}}{(p+\ell)!}\end{aligned}$$

utilizing the Jacobi-Anger expansion[1] we can perform the substitution of

$$\mathbf{42}\quad \sum_{\ell=-\infty}^{\infty}J_{\ell}\left(2\sqrt{2\kappa\zeta}\right)\exp\left(j\ell\left(2\pi\nu_x x+\phi\right)\right)\equiv\exp\left(j2\sqrt{2\kappa\zeta}\sin\left(2\pi\nu_x x+\phi\right)\right)$$

applying identity back into Eq.41 yields,

---

[1] $\exp(j\cdot\exp(-jz\cdot\sin\theta))=\Sigma J_n(z)\exp(jn\theta)$

$$\exp(\zeta)\exp\left(j2\sqrt{2\kappa\zeta}\sin(2\pi\nu_x x+\phi)\right)=\ldots$$

43

$$\ldots\sum_{\ell=-\infty}^{\infty}\sum_{p=0}^{\infty}\exp\left(j\ell\left(2\pi\nu_x x+\phi\right)\right)\frac{2^{\ell/2}\kappa^{\ell/2}L_p^{\ell}(2\kappa)\zeta^{p+\ell/2}}{(p+\ell)!}$$

multiplying both sides with a Gaussian beam, $\exp(-\kappa)$, we finally obtain

$$\exp(-\kappa)\exp(\zeta)\exp\left(j2\sqrt{2\kappa\zeta}\sin(2\pi\nu_x x+\phi)\right)$$

44

$$=\sum_{\ell=-\infty}^{\infty}\sum_{p=0}^{\infty}\exp(-\kappa)\exp\left(j\ell\left(2\pi\nu_x x+\phi\right)\right)\frac{2^{\ell/2}\kappa^{\ell/2}L_p^{\ell}(2\kappa)\zeta^{p+\ell/2}}{(p+\ell)!}$$

One may notice that the RHS (right hand side) sum member of Eq.44 is in fact the Laguerre-Gauss waveform at $z=0$, for $\ell\in\square$, using Eq.23 for this waveform, we may rewrite,

45 $$\text{RHS}=\sum_{\ell=-\infty}^{\infty}\sum_{p=0}^{\infty}\left[\begin{array}{l}\dfrac{1}{\sqrt{2p!\cdot(p+\ell)!}}\exp\left(j\ell 2\pi\nu_x x\right)\exp\left(j(2p+\ell)\pi\nu_y y\right)\times \\ \underbrace{\sqrt{\dfrac{2p!}{\pi w_0^2(p+\ell)!}}(2\kappa)^{\ell/2}\exp(-\kappa)L_p^{\ell}(2\kappa)\exp(j\ell\phi)}_{u_{\ell p}^{LG}(r,\phi,0)}\end{array}\right]$$

or, writing it with both sides explicitly, we get,

$$\exp(-\kappa)\exp(\zeta)\exp\left(j2\sqrt{2\kappa\zeta}\sin(2\pi\nu_x x+\phi)\right)=\ldots$$

46

$$\ldots=\sum_{\ell=-\infty}^{\infty}\sum_{p=0}^{\infty}\frac{1}{\sqrt{2p!\cdot(p+\ell)!}}\exp\left(j\ell 2\pi\nu_x x\right)\exp\left(j(2p+\ell)\pi\nu_y y\right)u_{\ell p}^{LG}(\kappa,\phi,0)$$

whereas,

$$u_{\ell p}^{LG}(r,\phi,0)=\sqrt{\frac{2p!}{\pi w_0^2(p+|\ell|)!}}\left(\frac{r\sqrt{2}}{w_0}\right)^{|\ell|}\exp\left(-\frac{r^2}{w_0^2}\right)L_p^{|\ell|}\left(\frac{2r^2}{w_0^2}\right)\cdot\exp(j\ell\phi)$$

or,

$$u_{\ell p}^{LG}(\kappa,\phi,0)=\sqrt{\frac{2p!}{\pi w_0^2(p+|\ell|)!}}(2\kappa)^{|\ell|/2}\exp(-\kappa)L_p^{|\ell|}(2\kappa)\cdot\exp(j\ell\phi)$$

This result, of Eq.44 is very important as it suggests that using a phase-mask of Eq.43 LHS (which is easy to realize), we may expect a waveform that consists of a superposition of ALL the Laguerre-Gauss beam modes.

This also sheds light on how the far field of Eq.46 is going to look like, we will use all those results, and also simulations, to make such predictions, in the following chapter.

Chapter 4. Simulation approaches and implementations

Gaussian beam simulations

In order to simulate the waveforms of Chapter 3, and validate the simulation, we used MATLAB with signal processing considerations.

The first challenge was to successfully simulate the propagation of a Gaussian wave as in Eq.26, for,

$w_0 = 1[\text{mm}]$

$z = 0[\text{m}], 3[\text{m}], 6[\text{m}], 9[\text{m}], 12[\text{m}], 15[\text{m}]$

$\lambda = 635[\text{nm}]$

The *aliasing* phenomenon, would subject the simulated waveform to get "stepped on" by it's replicas (which stems from discretizing the Fourier Transform) and therefore, become a different waveform.

Utilizing *Nyquist-Shannon sampling theorem* in a version applicable to finite space signals, we must first evaluate the *effective bandwidth* of the waveform, it can be done by finding it's Fourier transform and then calculate it's spectral width (which is the 2nd moment of it's intensity UU^*).

The bandwidth calculation is well documented in another source[viii], the result is, $B_x = \sqrt{\left(\frac{1}{\pi w(z)}\right)^2 + \left(\frac{w(z)}{\lambda R(z)}\right)^2}$,
where those parameters were explicitly explained in Table 3.

According to *Nyquist-Shannon sampling theorem*, we would like the sampling frequency to satisfy, $f_s > 2B_x$

Also, we would like to be able to see at least one spectral bandwidth of the Gaussian, therefore we choose the samples grid (L) to be greater than $w(z)$.

In this attempt, we used both Eq.19 in the code, and then Eq.27 in order to validate the result, as the former will be used exclusively from now on, where the latter will not be available for the more complex waveforms we would discuss.

Simulating the propagation of a Gaussian beam (Eq.19), we obtained Table 4, we used $E_0 = 5[V/m]$, the intensity was calculated by $|u|^2$, and the phase was obtained by $\angle u$.

The colorbar and the axes were omitted as the goal of table 6 was only to make comparisons and check validity, using the same MATLAB code, the energy ratio of both Eq.27 and Eq.19 was a unity, in agreement with energy conservation laws (Energy was calculated by $\int\int |u|^2 \, dxdy$).

The only apparent difference, was of that of the phases seem different, however, they aren't as the only interest in the phases is their pattern.
It seems that as we look further from the middle of the phase, the pattern becomes more dense, this is due to the parabolic phase contributed to the wave by Eq.19 and governed by $R(z)$.

From the last paragraph we conclude, that Eq.19 and Eq.27 agree perfectly, and hence, Eq.19 provides a reliable tool of simulation, establishing that, we will from now on omit simulation information from the figures themselves, and use Eq.19 exclusively as it's able to simulate any waveform propagation, unlike Eq.27 which is only able to make predictions about Gaussian beams.

Table 4 was produced by the code of,
`Two_dimensional_Gaussian_beam_simulation_OUT_combined.m`

Table 4: an abstract comparison between Gaussian beam simulations, horizontal axis is *x*, vertical axis is *y*; columns from left to right: distance of propagation, intensity by Eq.27, intensity by Eq.19, phase by Eq.27, phase by Eq.19.

At distance	Intensity by Eq.27 (analytical)	Intensity by Eq.19 (numerical)	Phase by Eq.27 (analytical)	Phase by Eq.19 (numerical)
$z=0$	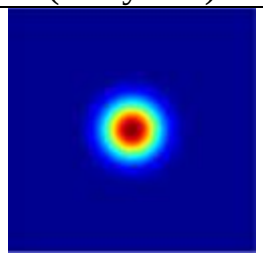	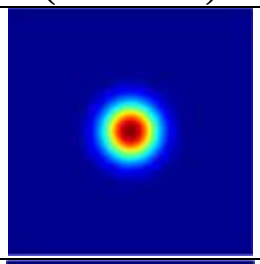	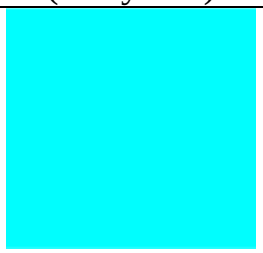	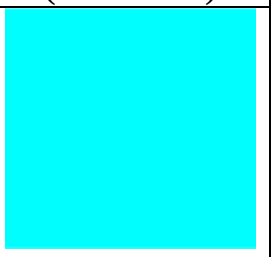
$z=3[m]$	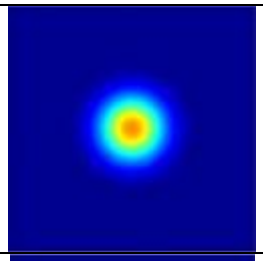	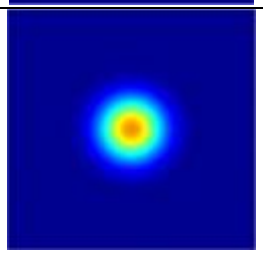	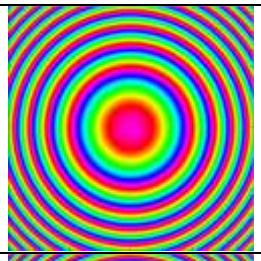	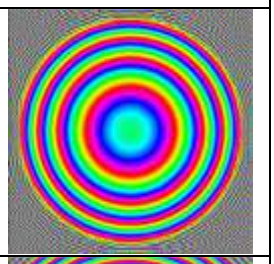
$z=6[m]$	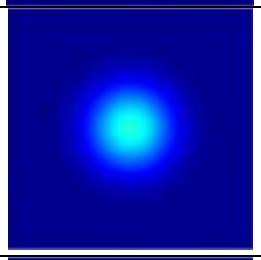	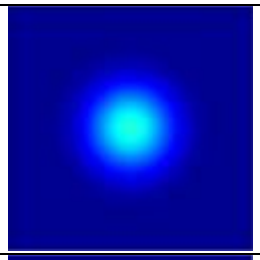	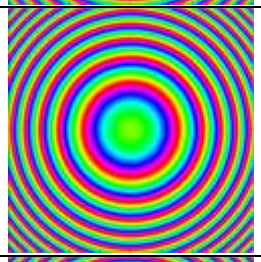	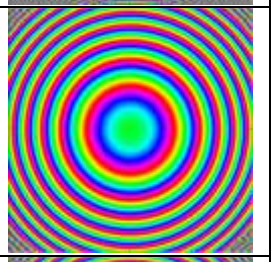
$z=9[m]$	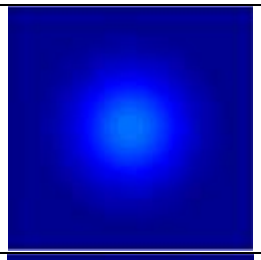	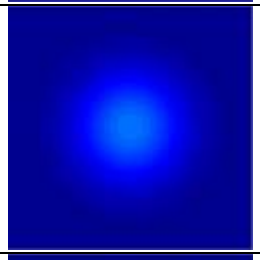	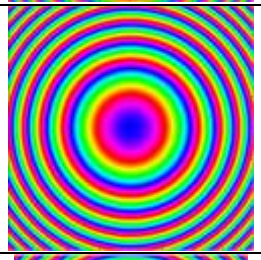	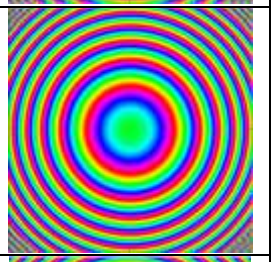
$z=12[m]$	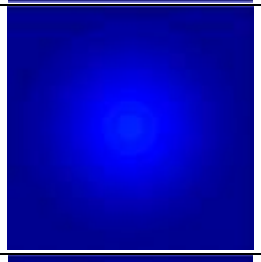	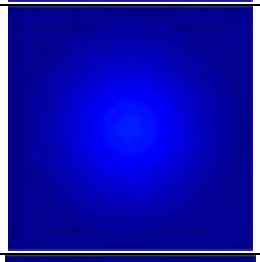	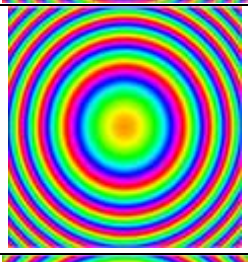	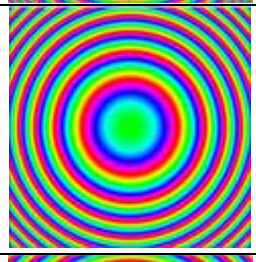
$z=15[m]$	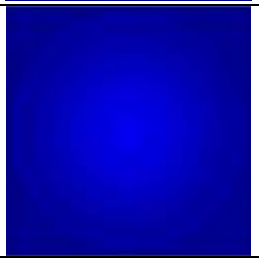	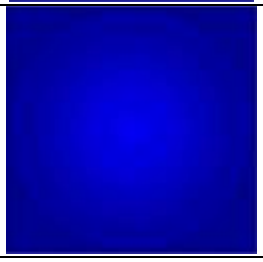	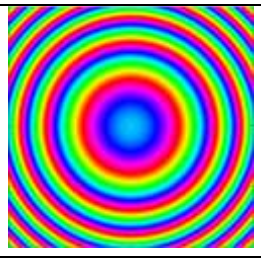	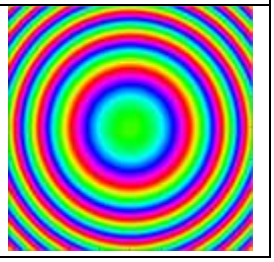

Laguerre-Gaussian beam modes simulations

As described in chapter 3, the Laguerre-Gaussian beam is given by Eq.23, we will reintroduce it here is a reminder,

$$u_{\ell p}(r,\phi,z)=\left[\begin{array}{l}\dfrac{C_{\ell p}^{LG}}{w(z)}\left(\dfrac{r\sqrt{2}}{w(z)}\right)^{|\ell|}\exp\left(-\dfrac{r^2}{w^2(z)}\right)L_p^{|\ell|}\left(\dfrac{2r^2}{w^2(z)}\right)\cdot \\ \exp\left(-jk\dfrac{r^2}{2R(z)}\right)\exp(j\ell\phi)\exp\left[j\left(2p+|\ell|+1\right)\zeta(z)\right]\end{array}\right]$$

It is, as discussed in chapter 3, an eigen-function (in respect to intensity), of the Paraxial wave equation, where cylindrical symmetry is in effect.

The first challenge (simulation-wise) is to get the formulas of the Laguerre-Polynomials themselves.

Fortunately, since MATLAB R2014b, there is a special built-in function, `laguerreL(n,a,x)`.
By using it, we can verify the first 4 Generalized Laguerre polynomials ($L_n^{\alpha}(x)$), and those are presented in Table 5.

Table 5: The first 4 Generalized Laguerre Polynomials, in their MATLAB symbolic functions, compared to the theoretical ones.

n	`laguerreL(n,a,x)`	3.21
0	`1`	1
1	`a - x + 1`	$-x+\alpha+1$
2	`(3*a)/2 - x*(a + 2) + a^2/2 + x^2/2 + 1`	$\dfrac{x^2}{2}-(\alpha+2)x+\dfrac{(\alpha+2)(\alpha+1)}{2}$
3	`(11*a)/6 - x*(a^2/2 + (5*a)/2 + 3) + x^2*(a/2 + 3/2) + a^2 + a^3/6 - x^3/6 + 1`	$-\dfrac{x^3}{6}+\dfrac{(\alpha+3)x^2}{2}-\dfrac{(\alpha+2)(\alpha+3)x}{2}+\dfrac{(\alpha+1)(\alpha+2)(\alpha+3)}{6}$

The next challenged we face is to use a simulation code in order to plot the intensity and phases of $\left\{u_{\ell p}(r,\phi;0)\right\}_{\ell,p=0}^{2}$ (Eq.23), meaning, the first 9 modes of the Laguerre-Gauss beam at input ($z=0$) plane.

The results are portrayed in Figure 5 and Figure 6.

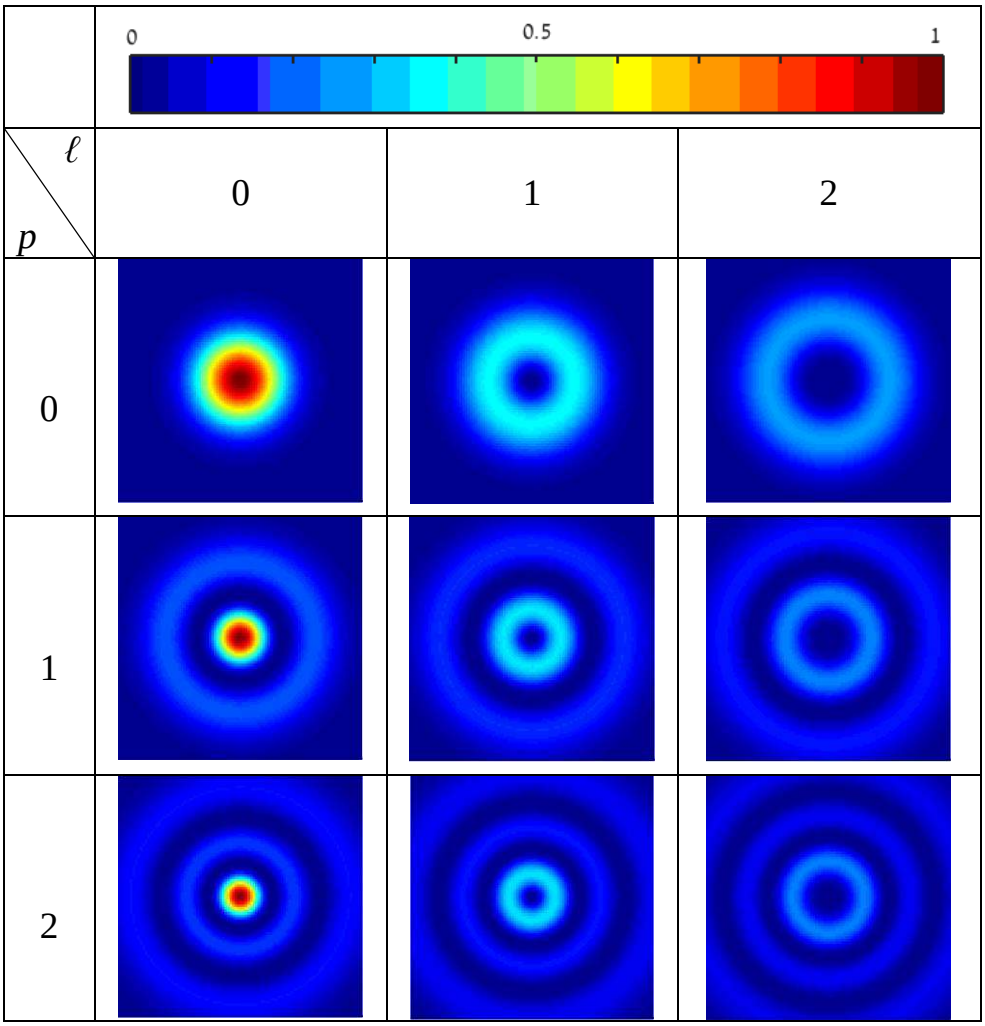

Figure 5: Intensity of the first 9 Laguerre-Gaussian beam modes, with waist[1mm], wavelength 635[nm], Rayleigh's length 4.9474[m], same metrical scale of measure for all figures.

Code used (requires at least MATLAB 2014b):
`Laguerre_Gaussian_modes_input_all_first_9_modes_intensity.m`

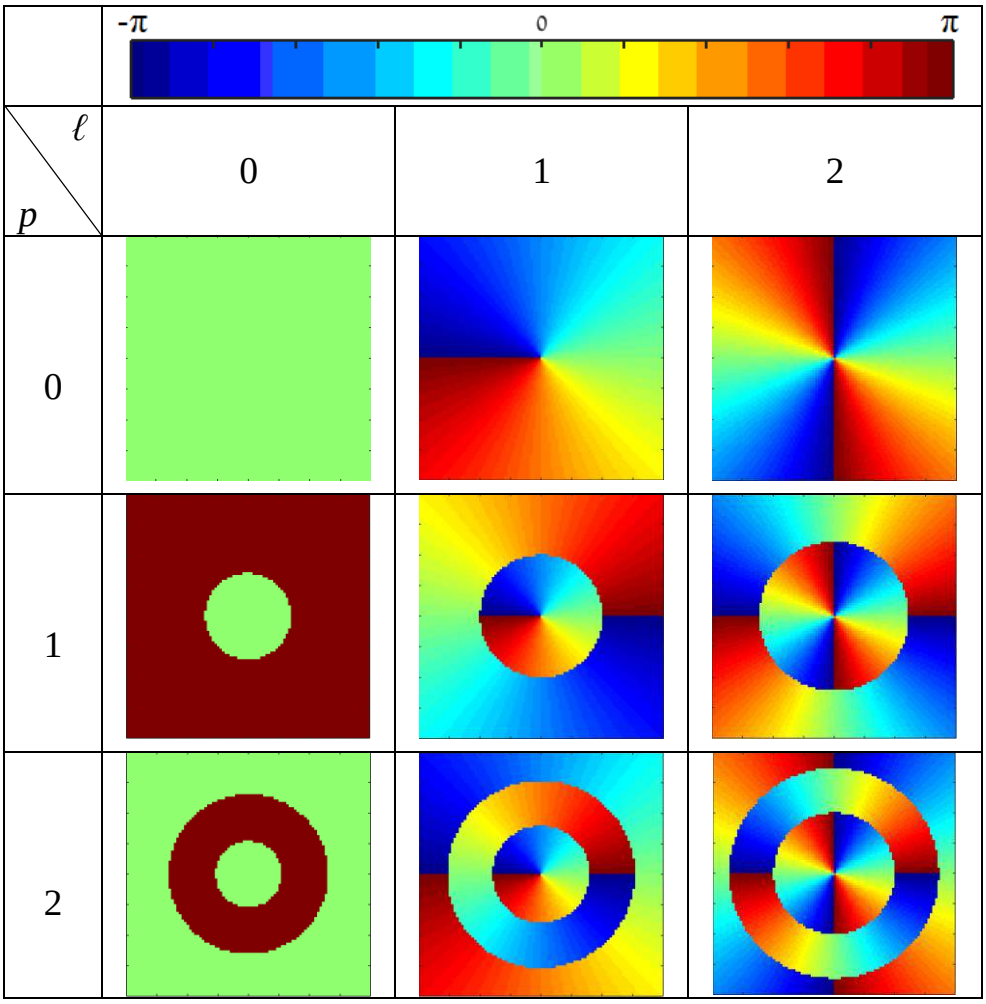

Figure 6: Phase of the first 9 Laguerre-Gaussian beam modes, with waist[1mm], wavelength 635[nm], Rayleigh's length 4.9474[m], same metrical scale of measure for all figures.

Code used (requires at least MATLAB 2014b):
`Laguerre_Gaussian_modes_input_all_first_9_modes_phase.m`

Figure 5 is pretty much easy to grasp as it depicts a multiplicity of a polynomial with a Gaussian, the rings formed in higher modes are contributed from the minima and maxima areas of the polynomials.

Figure 6 can be explained by the $\exp(j\phi\ell)$ factor in Eq.23.
It's name, *Angular Momentum*, is hijacked from Mechanics, and it causes a spiraling sweep of all angles allowed in ϕ.

On the p=0 order modes, the angular momentum is the exclusive phase factor and it's effect is depicted exclusively there, ℓ is the number of $[-\pi,\pi]$ periods depicted within the phase.

For p>0 modes, the phase is dependant on the the angular momentum, but also on the sign of the $L_p^{|\ell|}$ polynomials; when the sign of $L_p^{|\ell|}$ shifts, it causes and immediate shift of phase by a modulo π factor, hence the cones of p=1, that are contributed by the linear pattern of $L_1^{|\ell|}$ [1], and the toroids of p=2 orders which stem from the parabolic nature of $L_2^{|\ell|}$.

This phase analysis will be a key tool to understanding the more complex waveforms that will be simulated in the study.

[1] As seen in Table 5: The first 4 Generalized Laguerre Polynomials, in their MATLAB symbolic functions, compared to the theoretical ones.

Phase modulation Phase mask **– analysis by Jacoby-Anger Identity**

At this part of the study we aspired to create a simulation code that will, allow proper representation of Eq.32[1], and also inspect it's Angular Spectrum.

Given the discussion in Chapter 3, the waveform of $u_{00}(r)\exp(j\delta r\sin(2\pi v_x x-\phi))$ is a superposition of Gauss-Bessel modes, where those each of these modes is superposition of Gauss -Laguerre modes.

Regarding waveform at input plane (z=0[m])

Eq.32 has an obvious intensity of a Gaussian beam, and a phase of a phase-modulated sinusoidal wave in respect to x and ϕ, and as explained in the end of the Jacobi-Anger expansion theory, it creates variations in the instantaneous phase of the carrier wave.

Regarding waveform at far field plane (z>>0[m])

For the far field, we use Eq.20.

The intensity is given exclusively by the Fourier Transform of Eq.32, for that purpose we would examine the RHS (Right Hand side) of Eq.32.

The *Displacement* property of Fourier transforms dictates that a waveform, (in the xy plane) multiplied by a factor of $\exp(j2\pi v_x x)$, has the same Fourier Transform as the original wave, but shifted by v_x in respect to the horizontal axis.

Similar (but different) property applies when the waveform is multiplied by $\exp(j\delta r\sin(2\pi v_x x))$ as in Eq.20, the main difference is that multiple replicas of the original waveform ($u_{00}(r)$) will appear due to the periodic nature of a sine function, and they would have a reduced *Support* by $1/\delta$.

Given v_x is "large enough" to allow proper separations (of the replicas), using a variant of Eq.40 (same equation actually, just taking $-\phi$ instead of ϕ), we would expect for each n to see all the $\left\{u_{np}^{LG}(r,\phi;z)\right\}_{p=0}^{\infty}$ stacked (or converged) upon each other, and for each n to account for another stack of the above set (separated [by v_x] from the former set).

This pattern is expected to be infinite in the x axis, and by the discussion in chapter 3, in respect to intensity $\left\{u_{np}^{LG}(r,\phi;z)\right\}_{p=0}^{\infty}$ has the same shape as

---

[1] $u_{00}(r)\exp(j\delta r\sin(2\pi v_x x-\phi)) = \Sigma\, u_{00}(r)J_n(\delta r)\exp(-jn\phi)\exp(jn2\pi v_x x)$

$\left\{u_{np}^{LG}(r,\phi;0)\right\}_{p=0}^{\infty}$, as it's an eigen-function of Eq.19 and is given for a few modes in figures Figure 5 and Figure 6.

The Angular Spectrum phase aspect of Eq.32 is expected to show separated figures (again, assuming ν_x is large enough), with the linear phase of $\exp(jn2\pi\nu_x x)$, an angular momentum $\exp(-jn\phi)$ (spiraling phase), discontinuous step jumps from 0 to π dependant on $J_n(\delta r)$'s sign, and finally, a **parasitic** parabolic phase due to far-field (Eq.20) (could be removed using a lens).

Using the codes of,

```
Jacobi_anger_simulation_LeftHandSide_Propagation_differentCB.m
```

and,

```
Jacobi_anger_simulation_LeftHandSide_Propagation_SameClampedCB.m
```

the simulation produced outputs exactly as was predicted in last paragraph; those outputs are summarized in Figure 7.

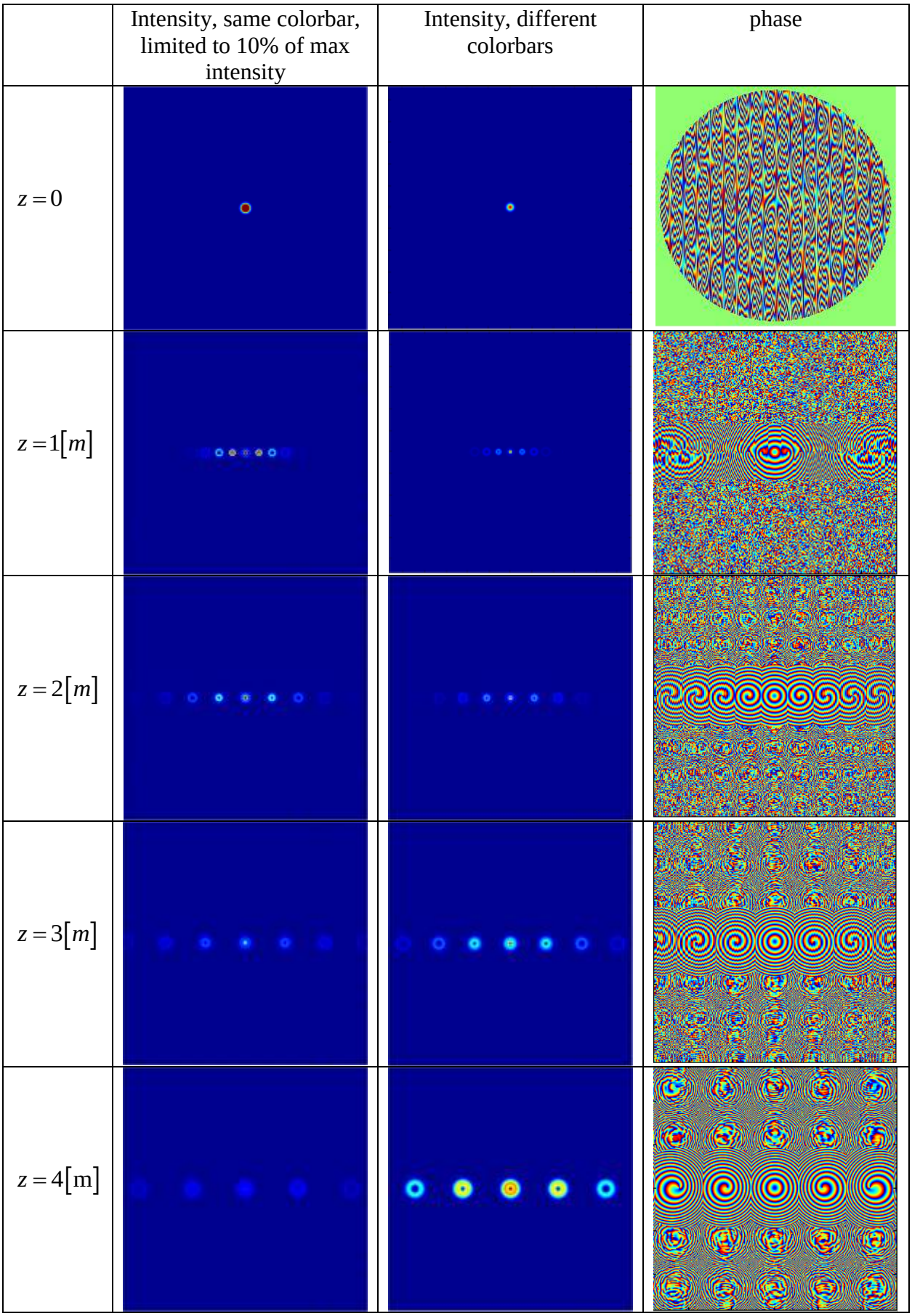

Figure 7: Eq.31's LHS, propagation to (top to bottom) z=0,1,2,3,4[m] (each row), columns from left to right, distance[m], intensity by the same colorbar clamped to 10% of maximum intensity, intensity by a different colorbar, phase. Grid size L=55*w(z=4[m]), sampling frequency f_s =75*B, w0=1mm, δ=50/(L/2), v_x=126/(L/2)

A necessary tool, to further ascertain the validity of Eq.31, is correlating the angular spectra of the LHS and RHS_n (*n* being the mode order for each member in the RHS sum).
The correlation' ($\Im\{LHS \cdot RHS_n^*\}$) intensity (or by the convolution theorem $\Im\{LHS\} \otimes \Im\{RHS_n^*\}$), is expected to give a distinct peak at the point the mode order (*n*) is present.
Not only is it a good validation tool, it is also the way an optical filter (with LHS's pattern) can demultiplex a multimode beam, as it does in Shoam Swartz study.

Wishing to simulate both the angular spectrum of $LHS \cdot RHS_n^*$, and it's far field.

We used the following code to accomplish former:
`Jacobi_anger_simulation_LeftHandSide_Corellation_LHS12.m`
as it's output is summarized in Figure 8.
The output agrees with the predictions made in last paragraph.

Upon learning that it's more elegant to show centered figures, we omitted (without harming the results) the displacement factor of the RHS of Eq.32[1] from the code of the far field correlation of the name:
`Jacobi_ANger_RHS_COR_LHS_FAR_FIELD.m`
where it's output can be seen in Figure 9.
The output agrees with the predictions made in last paragraph.

The main distinct difference between figures Figure 8 and Figure 9, is in the phase, this doesn't contradict the predictions as the far field (depicted in Figure 9) carries, as explained before, a **parasitic** parabolic phase as shown in Eq.20.

[1] $\exp(jn2\pi v_x)$

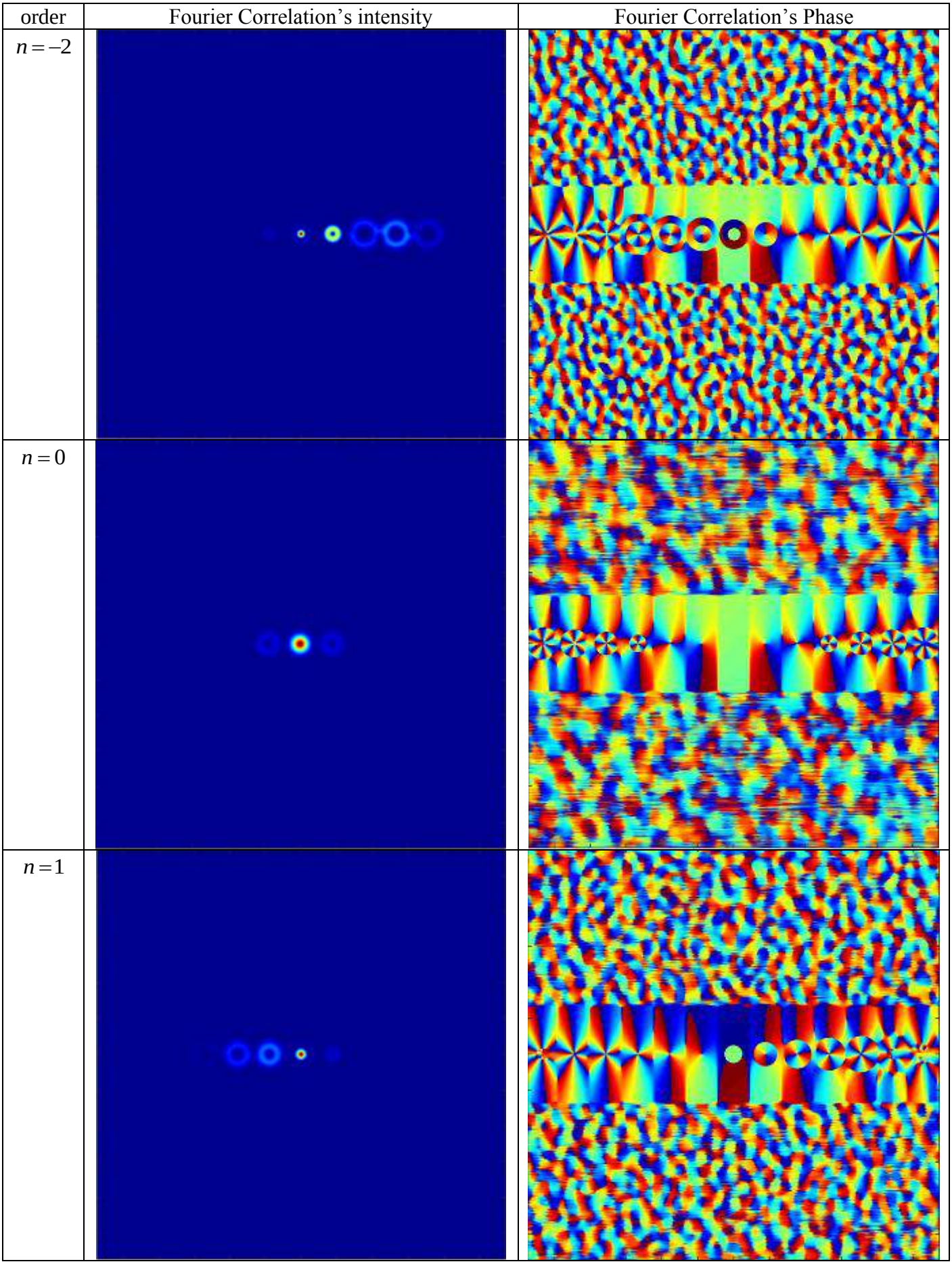

Figure 8: Correlations for the angular spectra of both Eq.31's LHS and a single sum member of it's RHS. From top to bottom, the order of the single sum member of the RHS, n=-2,0,+1 From left to right, the order of the RHS sum member, LHS&RHS$_n$'s angular spectra correlation intensity, LHS&RHS$_n$'s angular spectra correlation phase.
The above for parameters: Grid size L=90*w_0, sampling frequency f_s =90*B, w_0=5mm, δ=50/(L/2), v_x=100/(L/2).

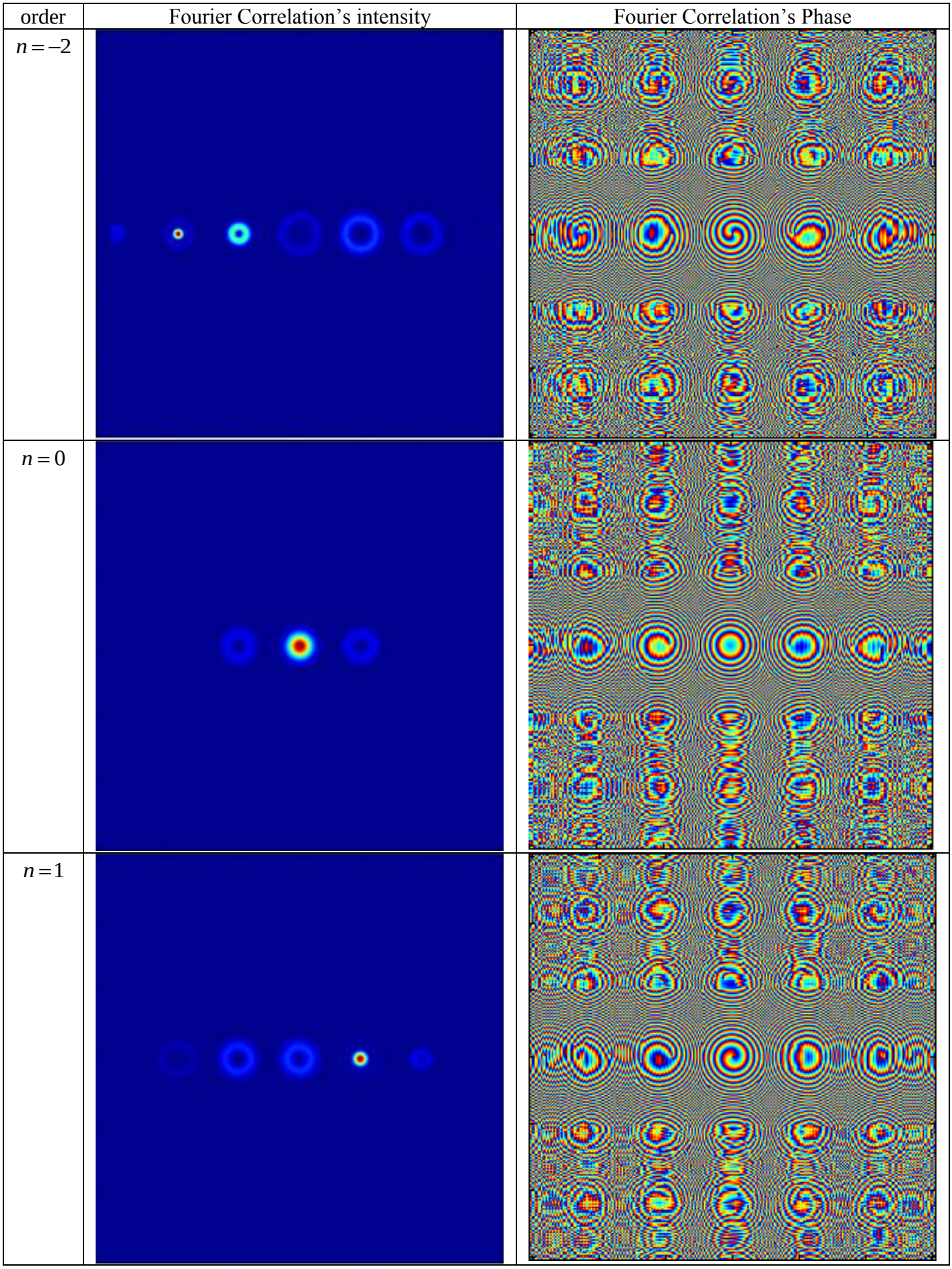

Figure 9: Correlations for the far fields of both Eq.31's LHS and a single sum member of it's RHS. From top to bottom, the order of the single sum member of the RHS, n= -2,0,+1. From left to right, the order of the RHS sum member, LHS&RHS$_n$'s far field correlation intensity, LHS&RHS$_n$'s far field correlation phase.
The above for parameters: Grid size L=90*w(z=4[m]), sampling frequency f_s =225*B, w_0=1mm, δ=50/(L/2), v_x=126/(L/2).

Bessel-Gaussian beams **– The *Single* and *Double* sum problems**

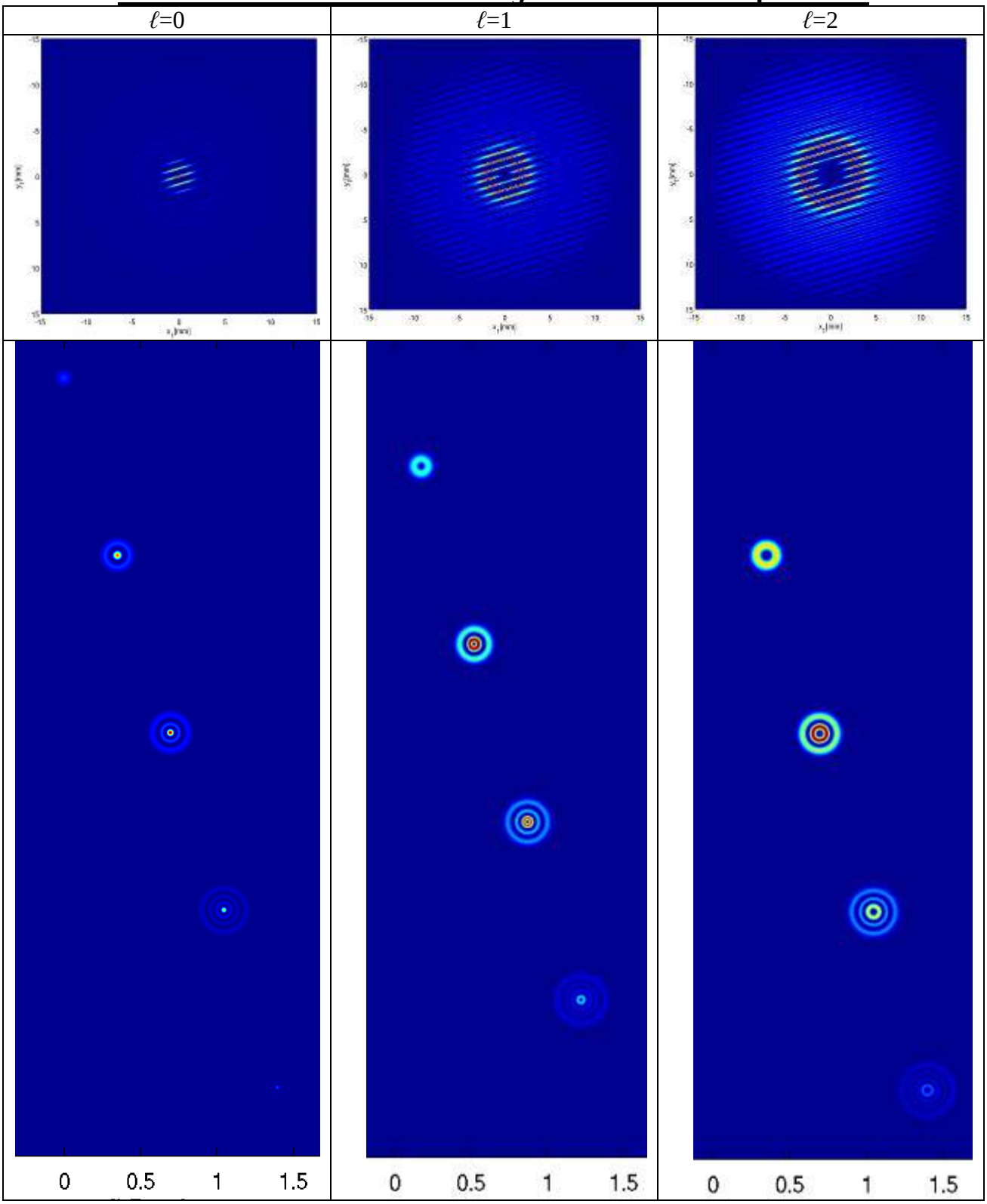

Gauss Bessel – Single sum intensity, angular spectra

order	Phase	Angular spectra Phase
ℓ=0	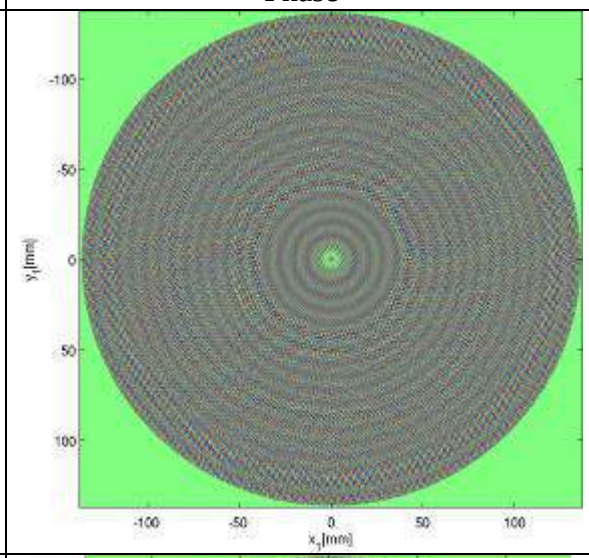	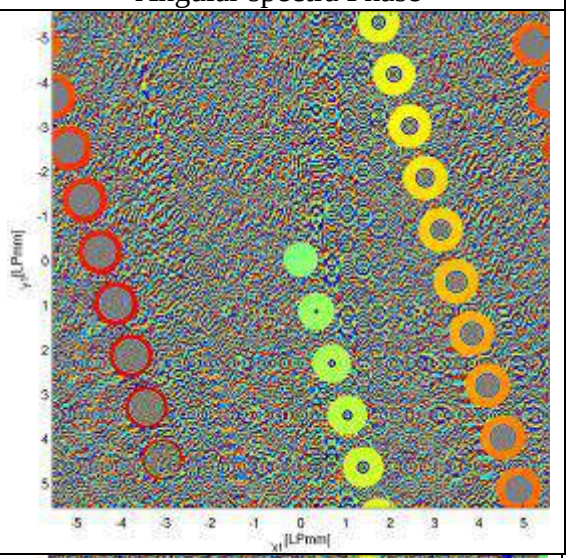
ℓ=1	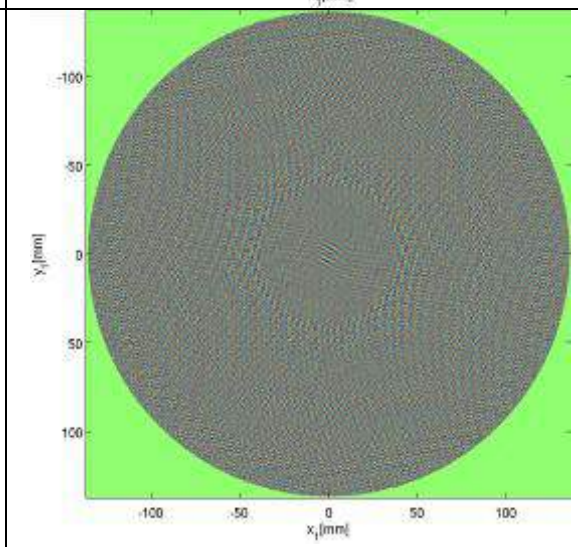	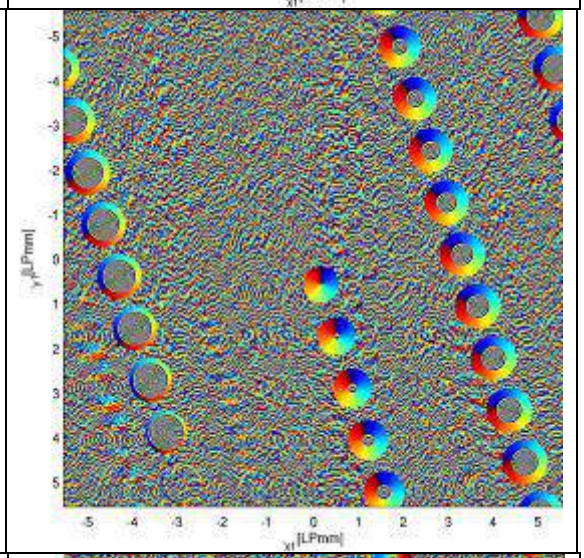
ℓ=2	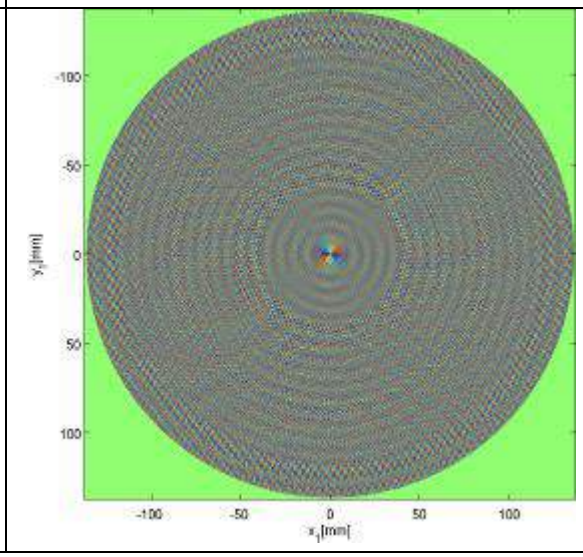	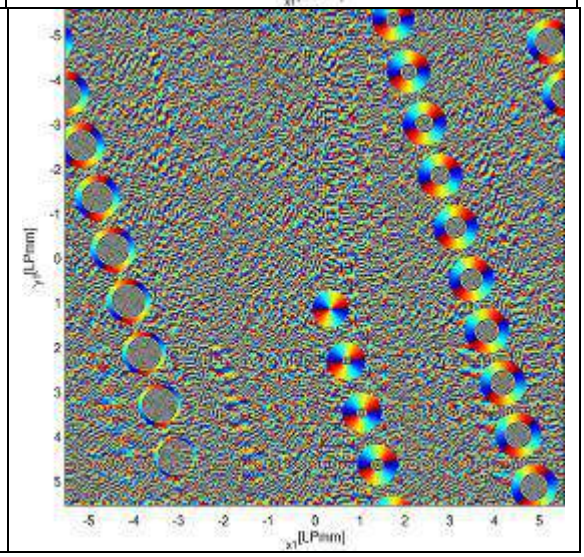

Gauss Bessel – Single sum intensity, angular spectra

ℓ /p	0	1	2	3
0	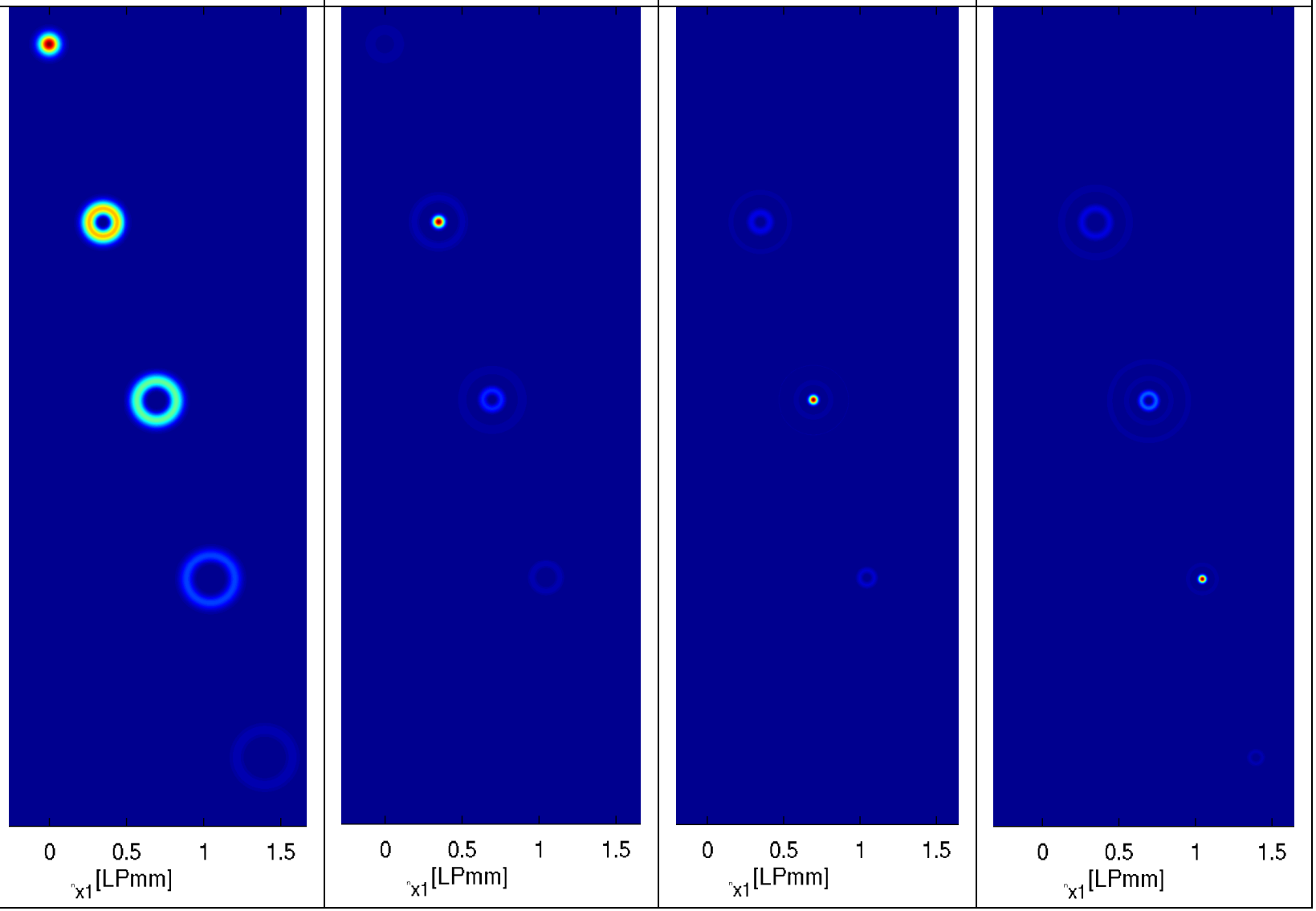			

Gauss Bessel Single Sum (Correlation) $\Im\left\{LHS\left(\ell\right)\cdot RHS^{\dagger}\left(p,\ell\right)\right\}$ **Intensity**, y&x axes are the spatial frequencies ν_y,ν_x in [LPmm]

	ℓ /p	0	1	2	3
	1	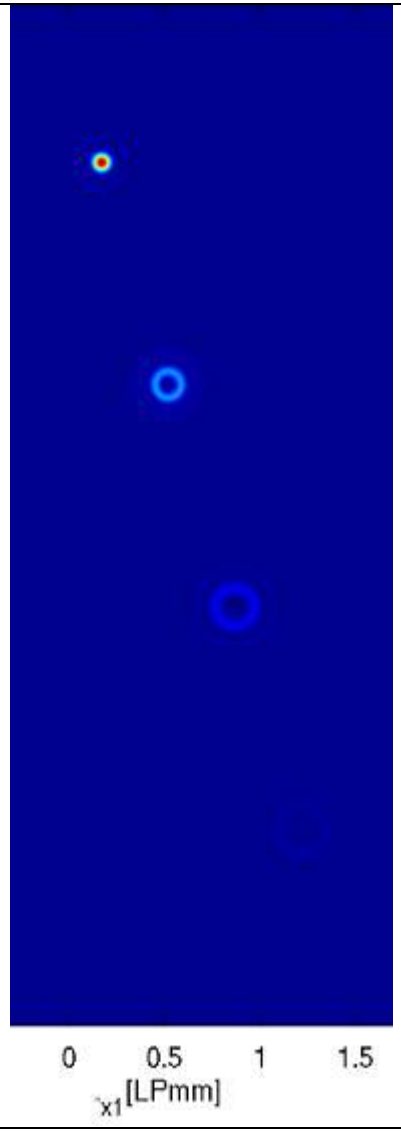	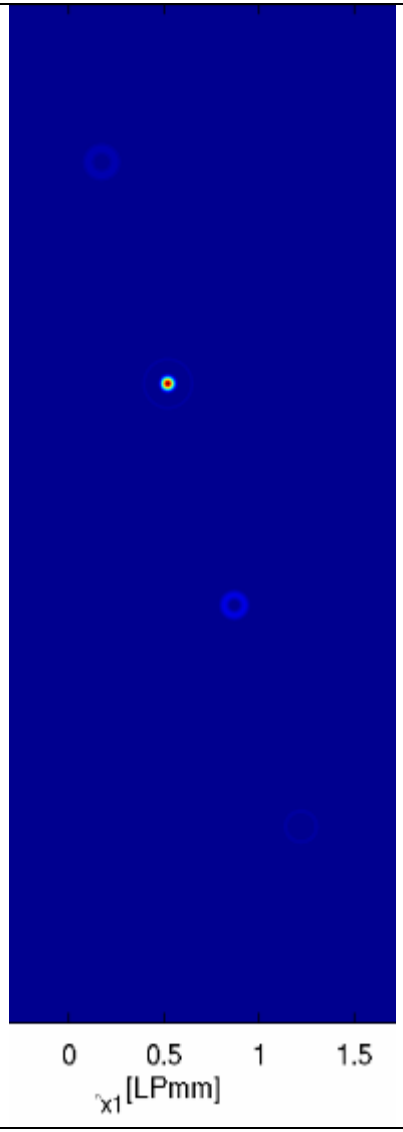	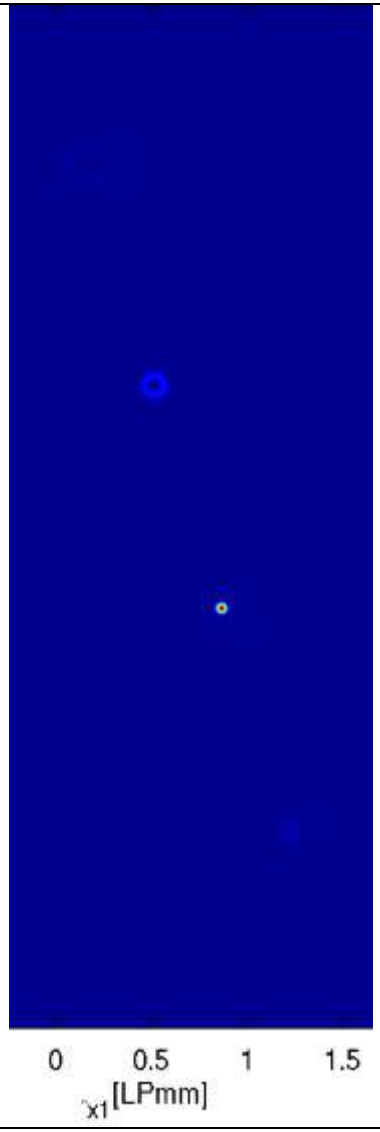	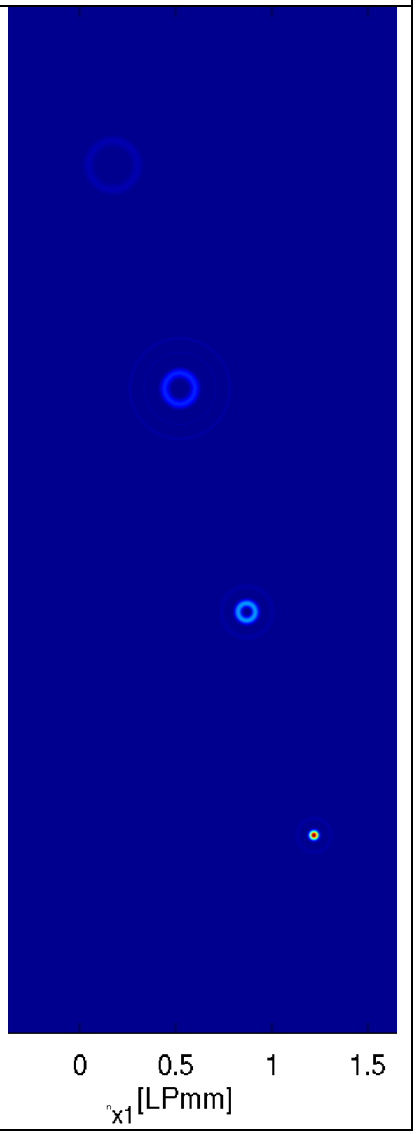

Gauss Bessel Single Sum (Correlation) $\Im\left\{LHS\left(\ell\right)\cdot RHS^{\dagger}\left(p,\ell\right)\right\}$ **Intensity**, y&x axes are the spatial frequencies ν_y,ν_x in [LPmm]

	ℓ /p	0	1	2	3
	2	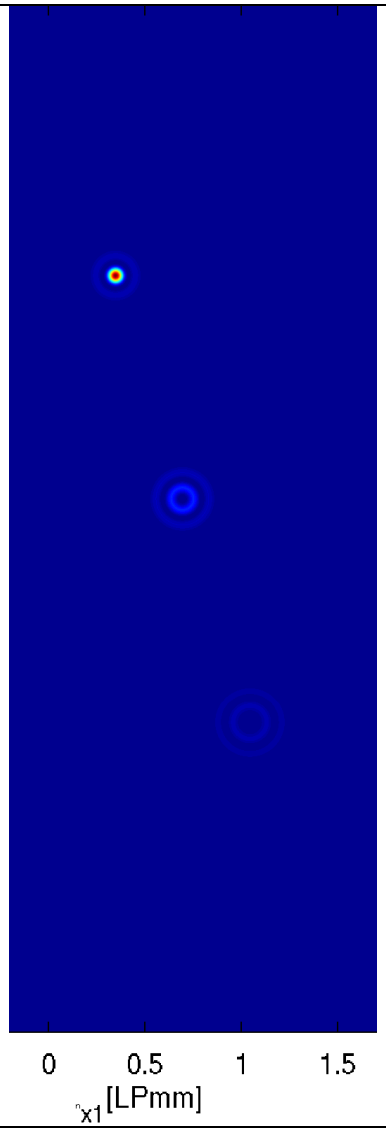	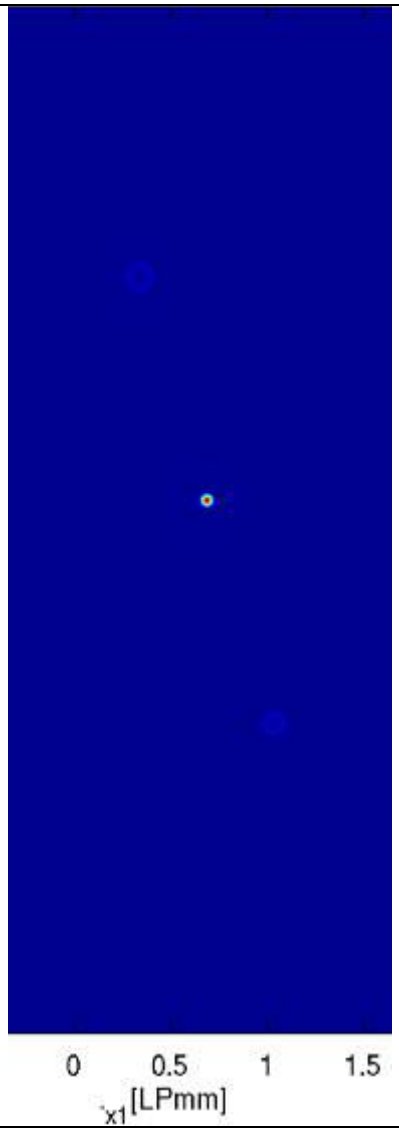	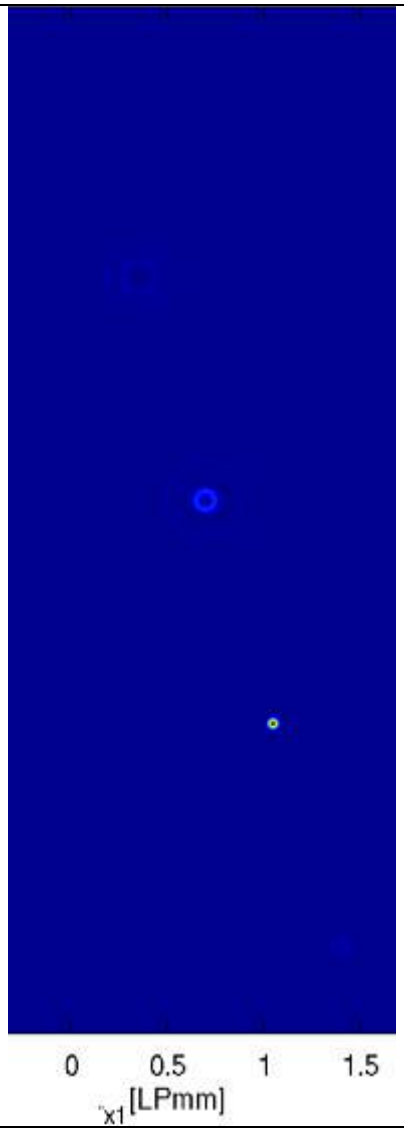	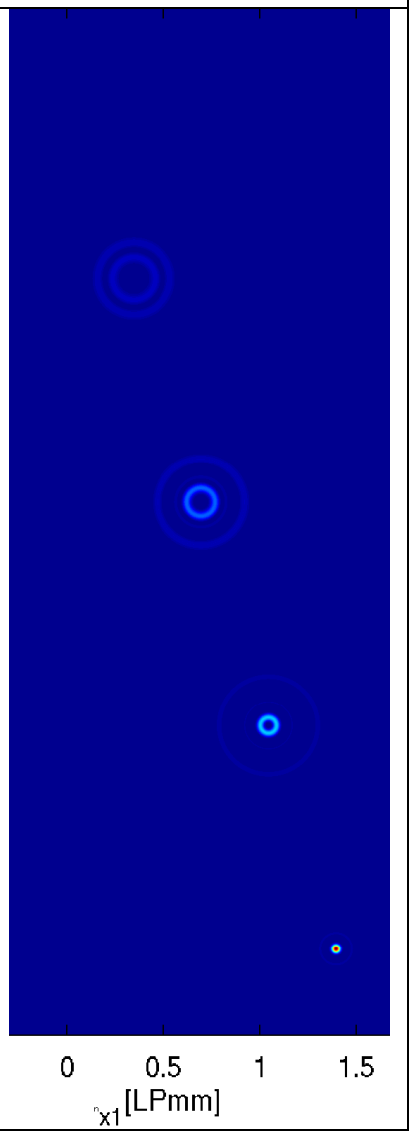

Gauss Bessel Single Sum (Correlation) $\Im\left\{LHS\left(\ell\right)\cdot RHS^{\dagger}\left(p,\ell\right)\right\}$ **Intensity**, y&x axes are the spatial frequencies ν_y,ν_x in [LPmm]

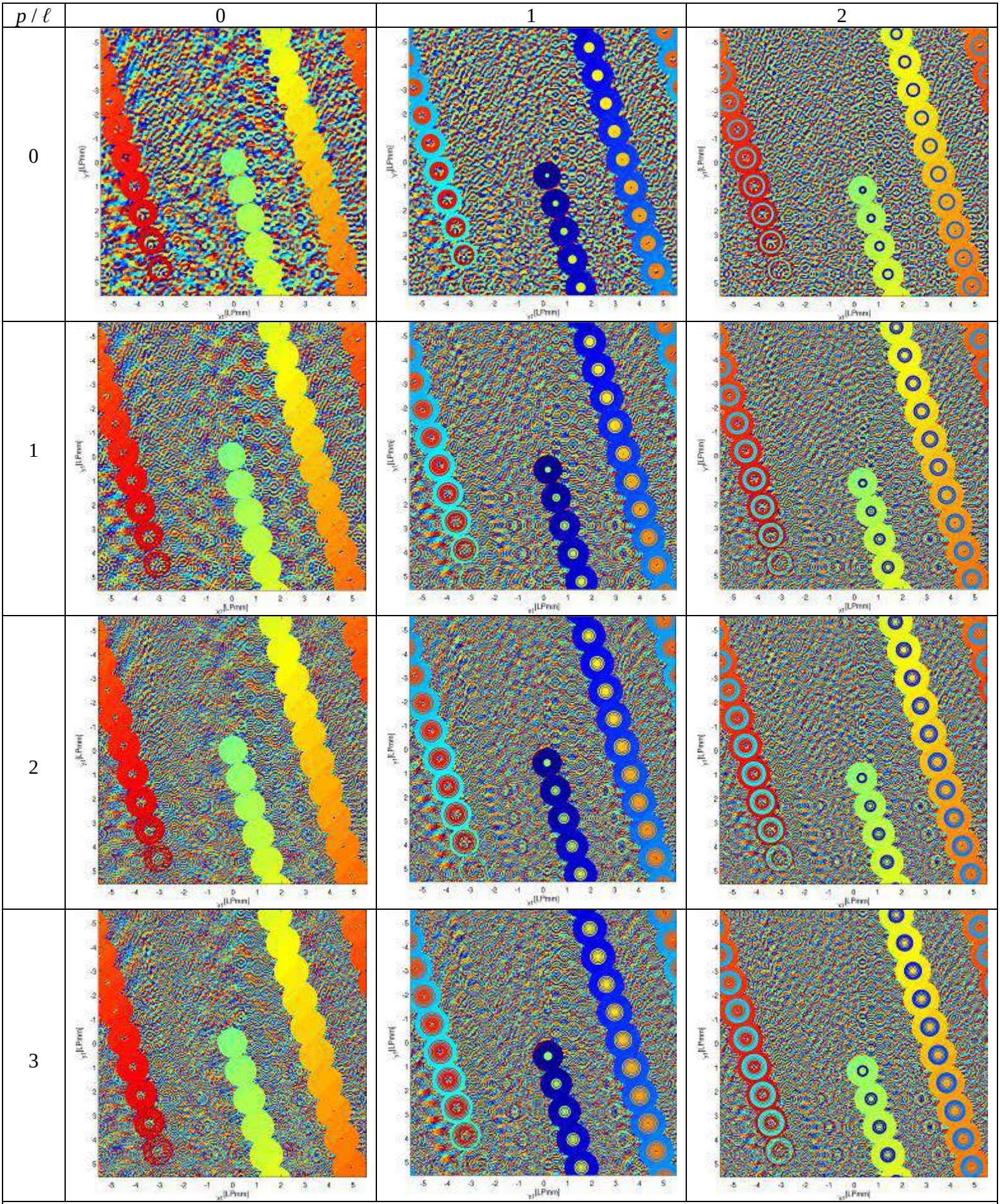

Fig Gauss Bessel Single Sum phase (Correlation)

Gauss-Bessel Double Sum

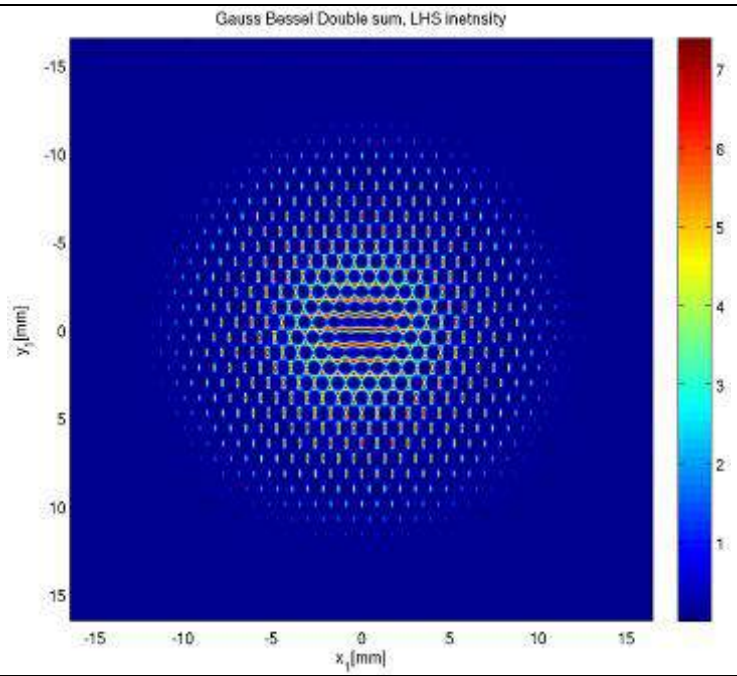

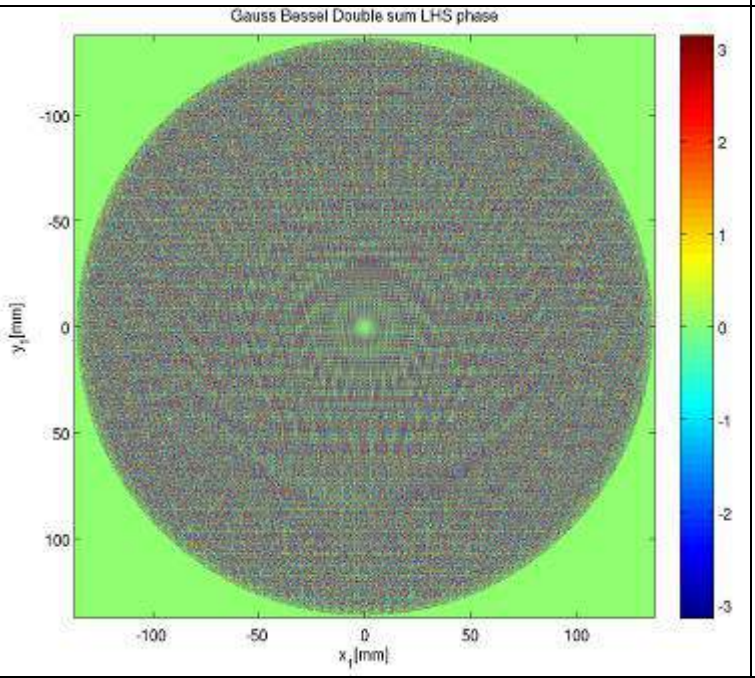

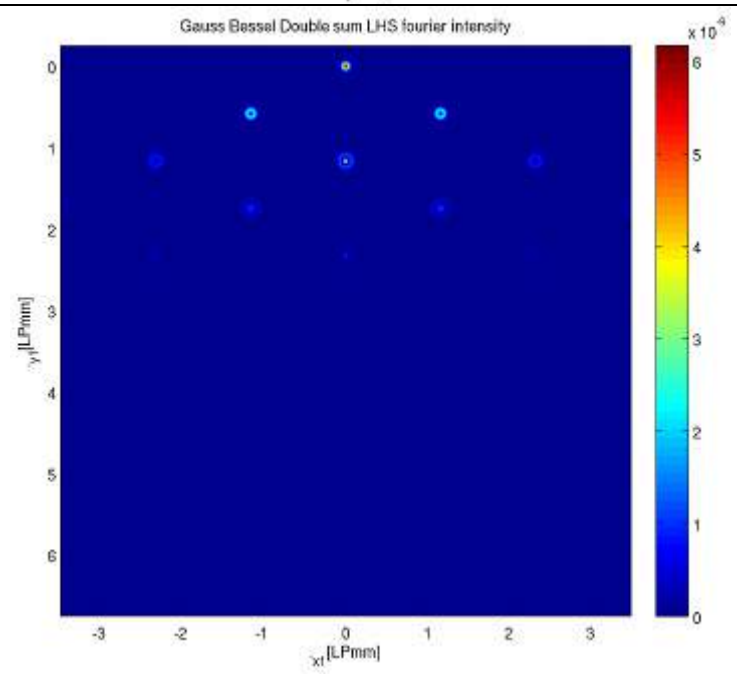

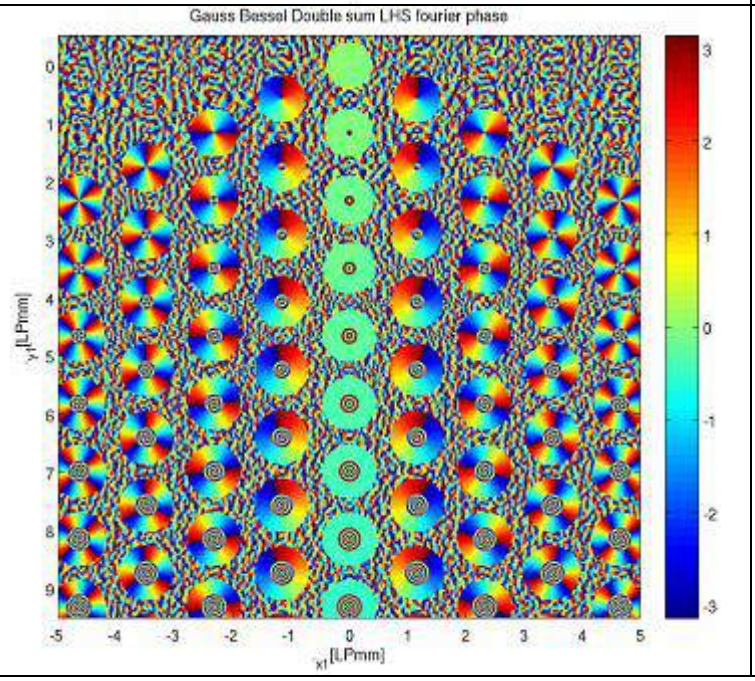

Gauss-Bessel Double Sum LHS, titles are on the graphs

	Cor Four Int	Cor Four phase
ℓ / p	0	
0	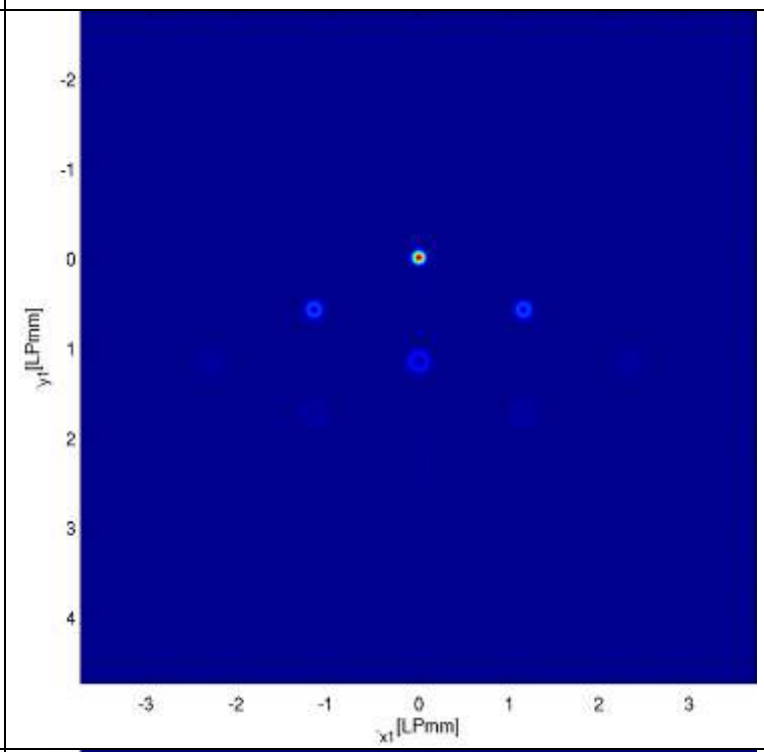	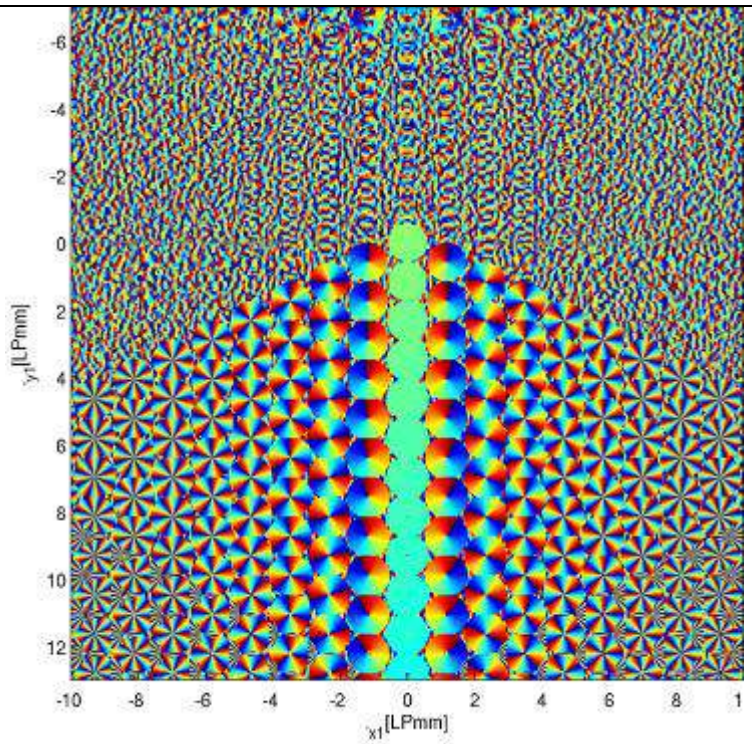
1	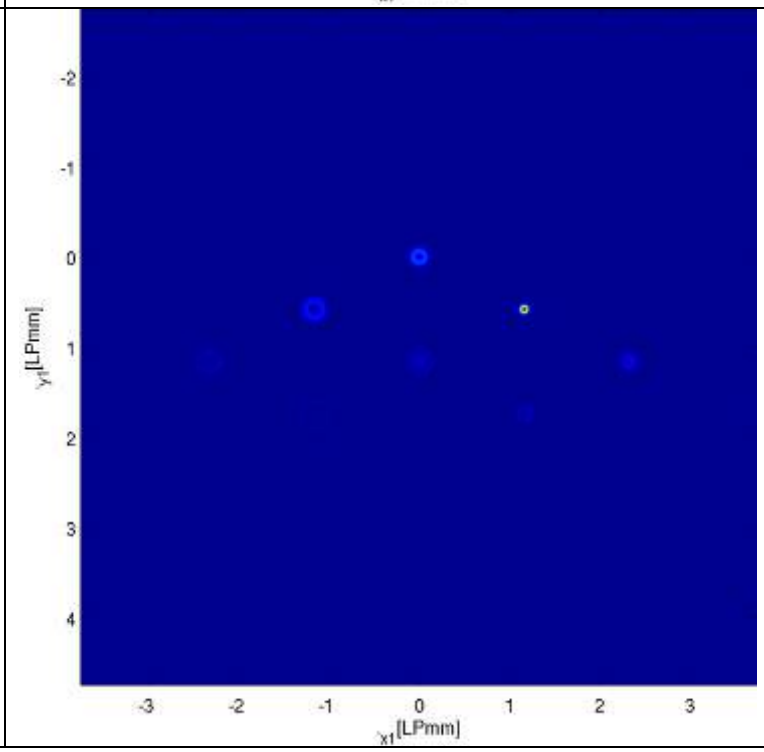	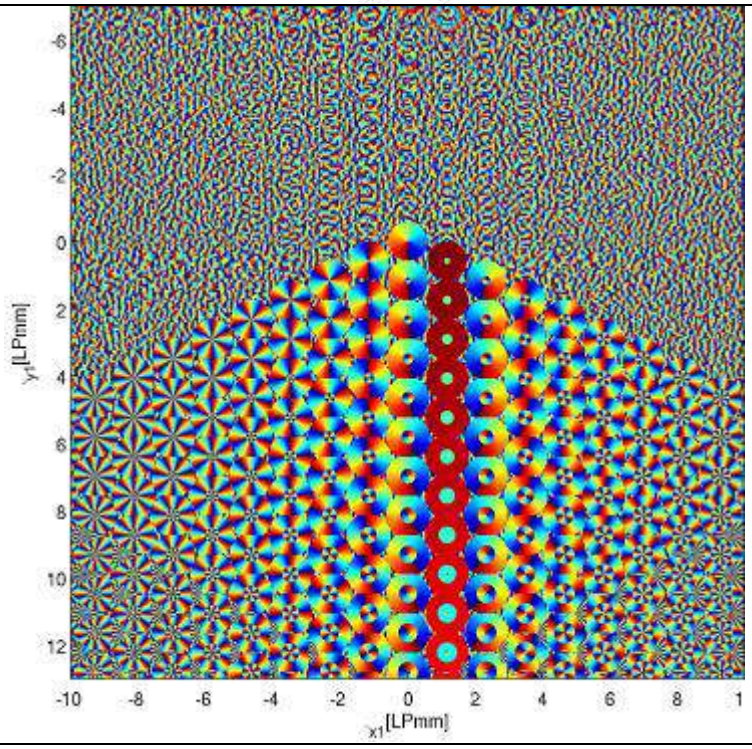

Gauss-Bessel Double Sum correlation

	Cor Four Int	Cor Four phase
ℓ / p	0	
-2	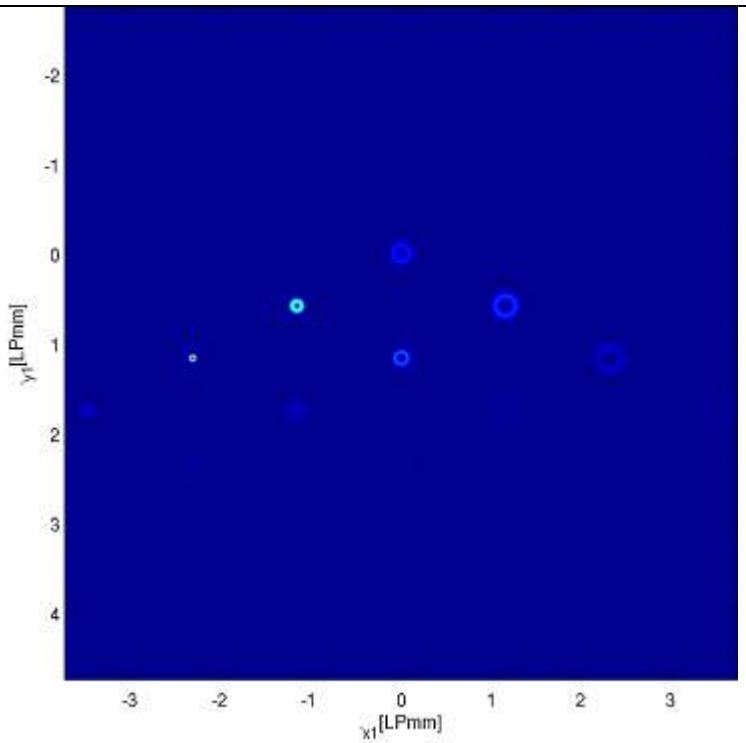	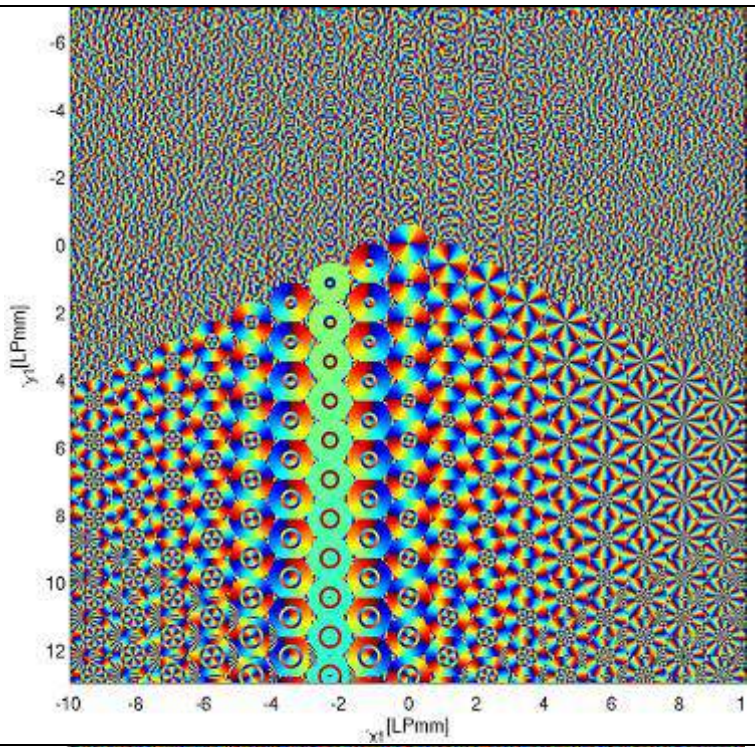
3	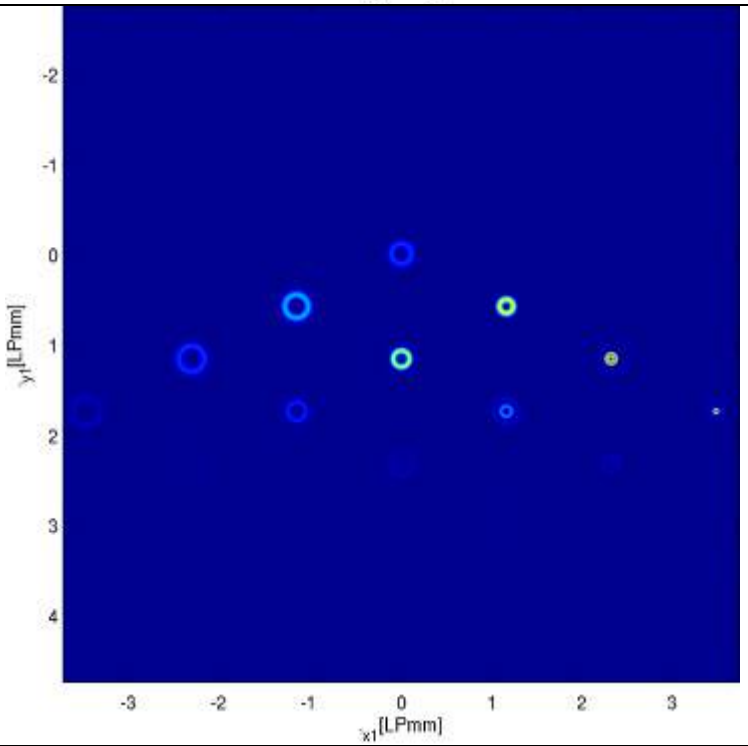	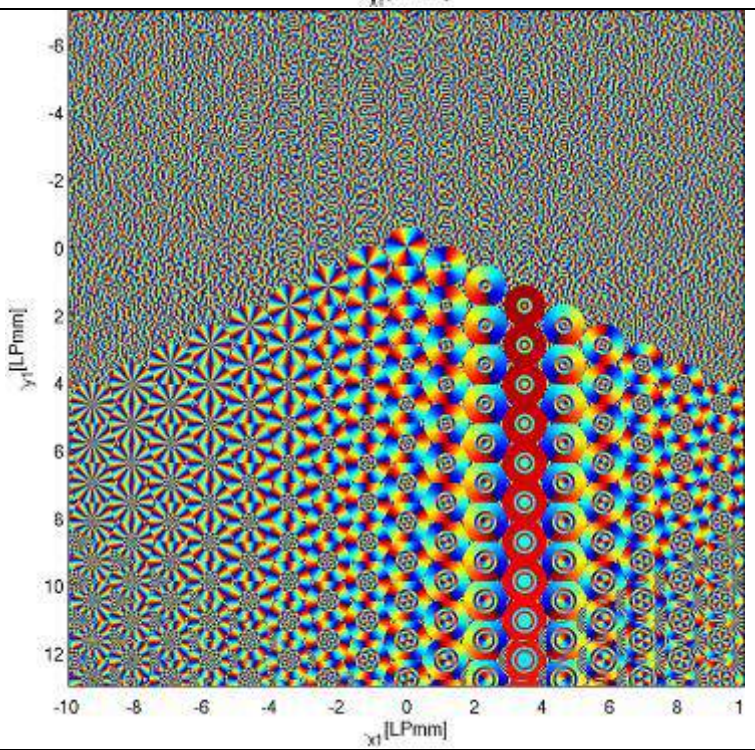

Gauss-Bessel Double Sum correlation

	Cor Four Int	Cor Four phase
ℓ / p	1	
0	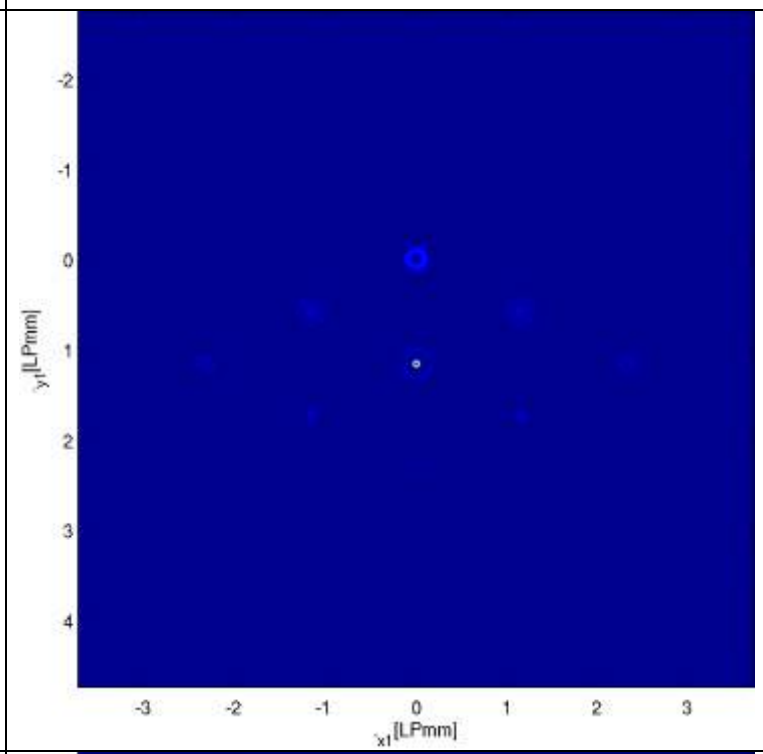	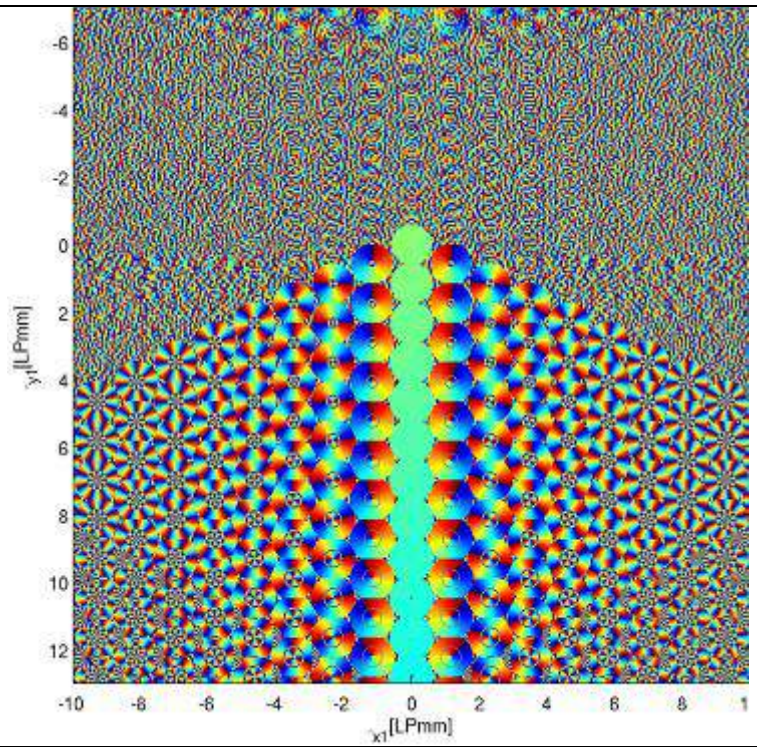
1	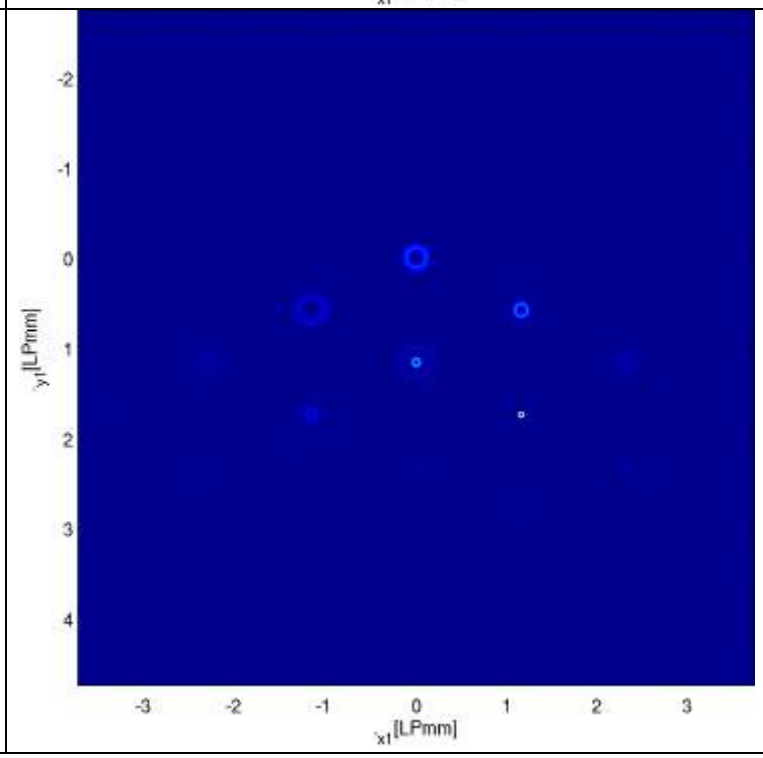	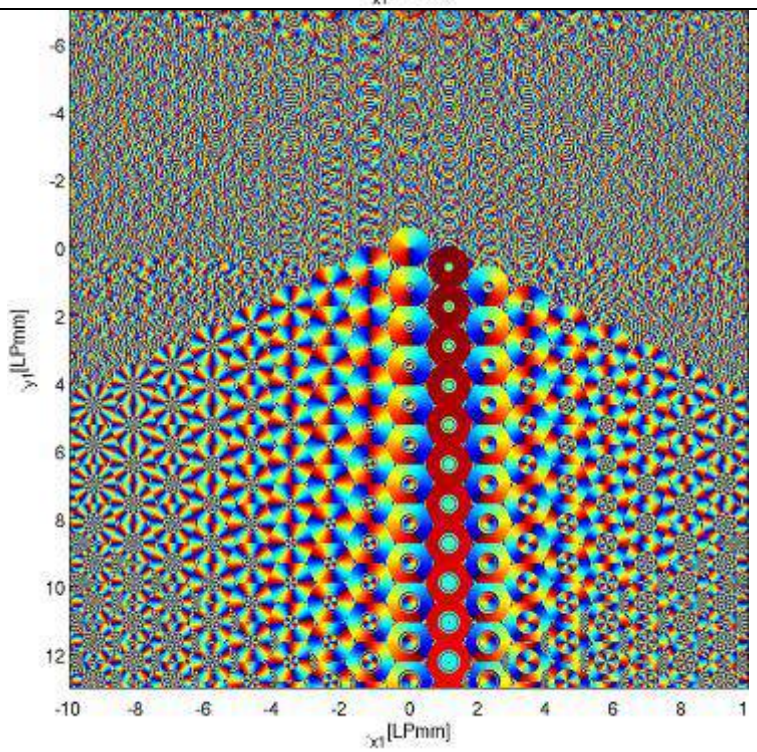

Gauss-Bessel Double Sum correlation

	Cor Four Int	Cor Four phase
ℓ / p	1	
-2	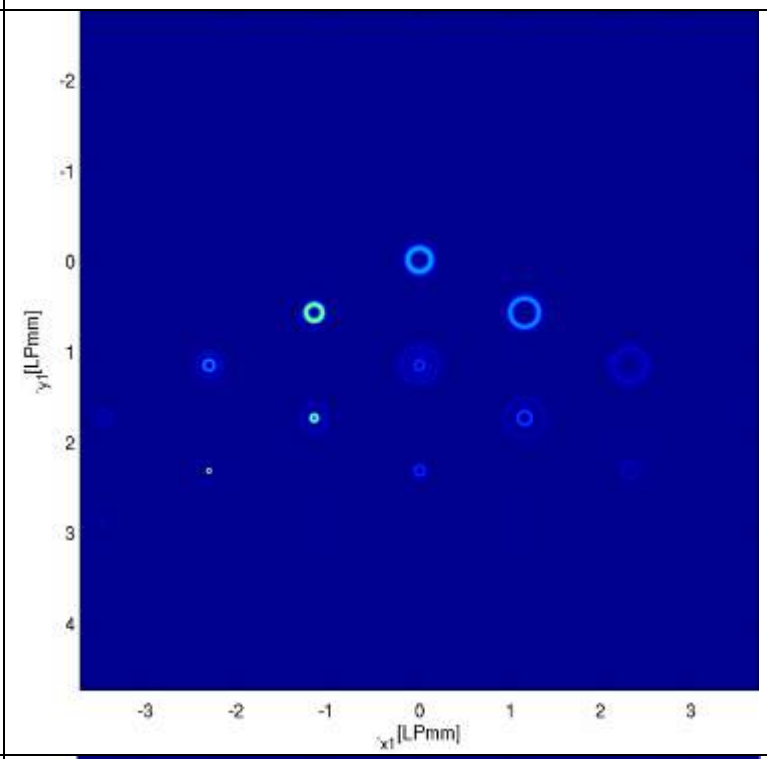	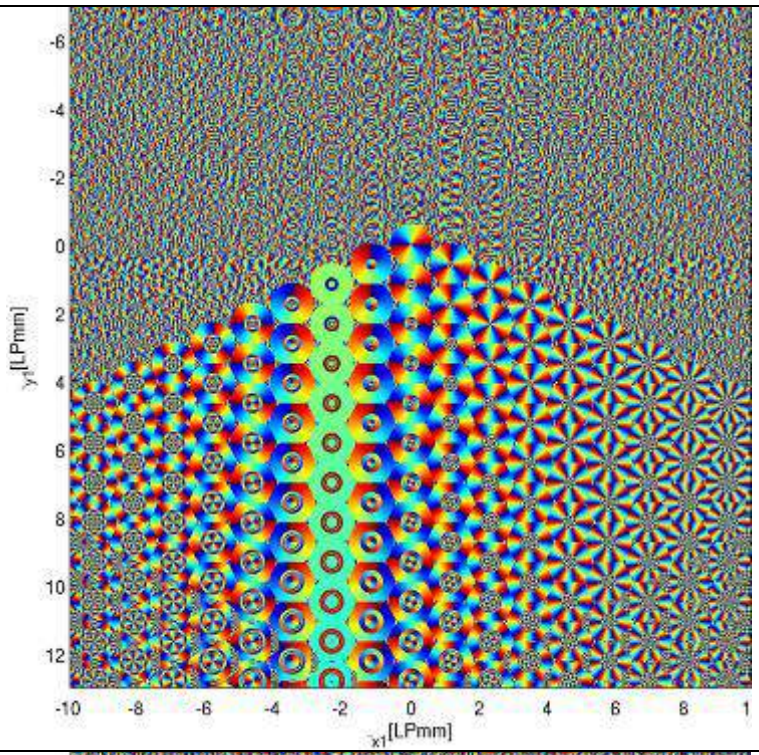
3	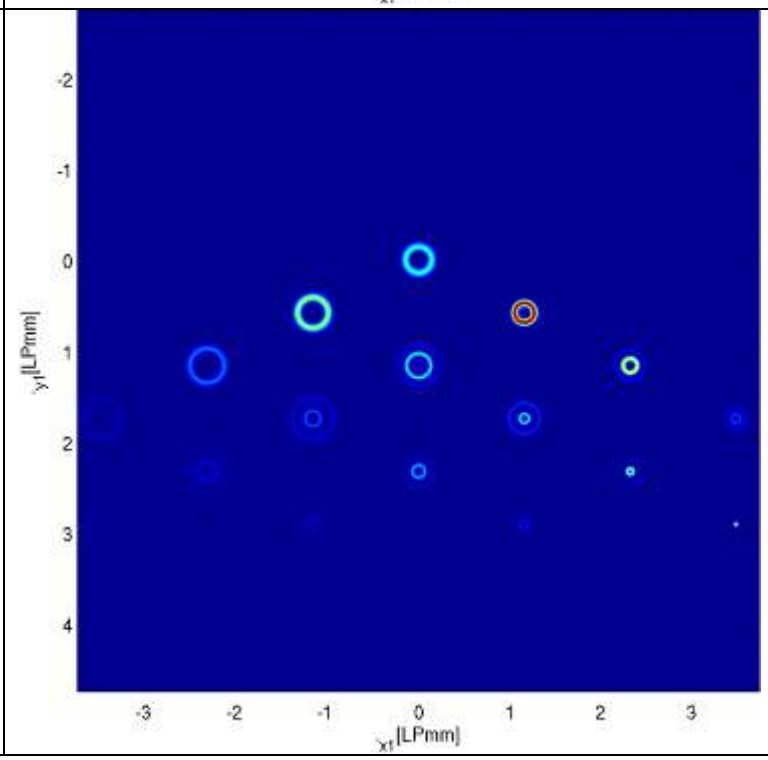	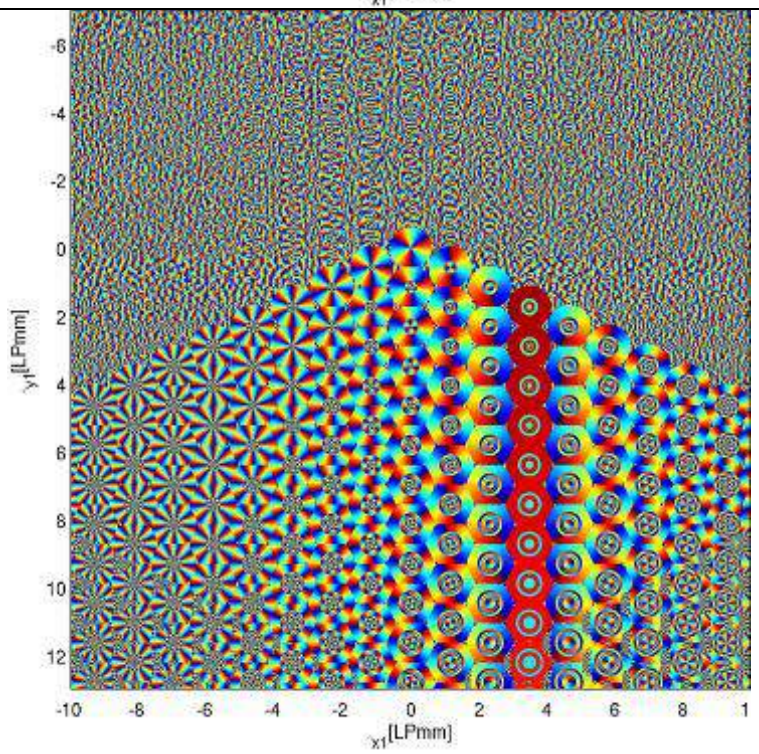

Gauss-Bessel Double Sum correlation

	Cor Four Int	Cor Four phase
ℓ / p	2	
0	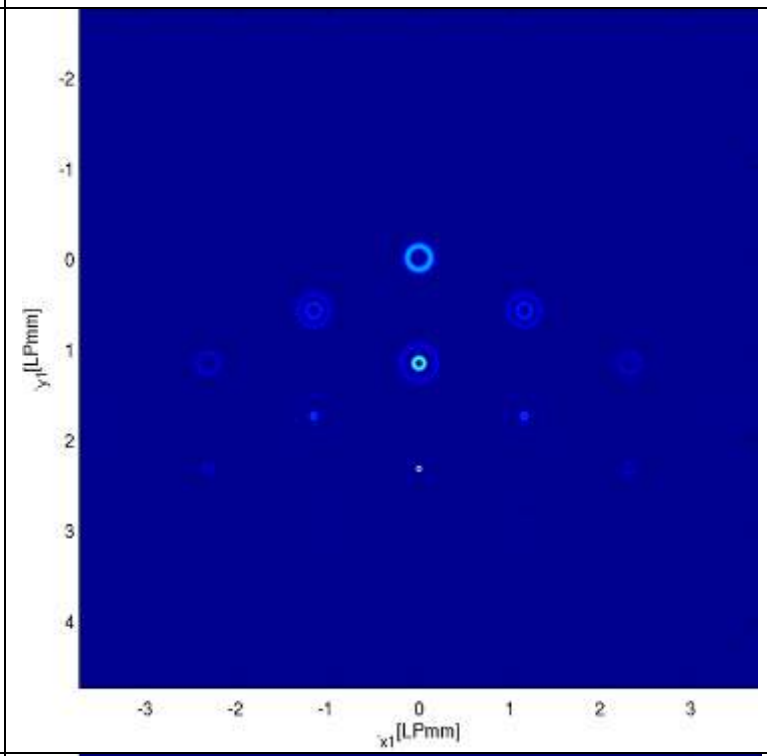	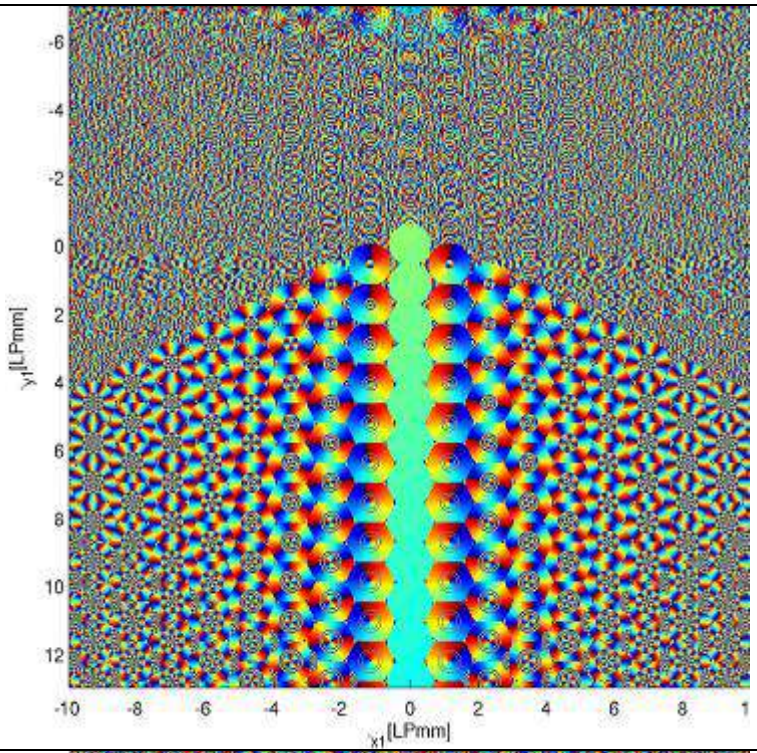
1	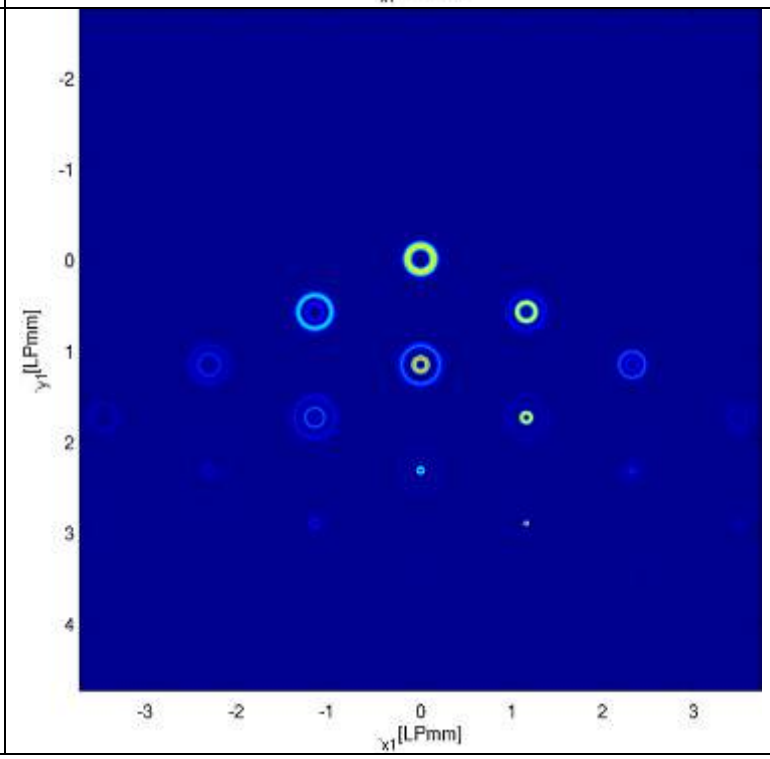	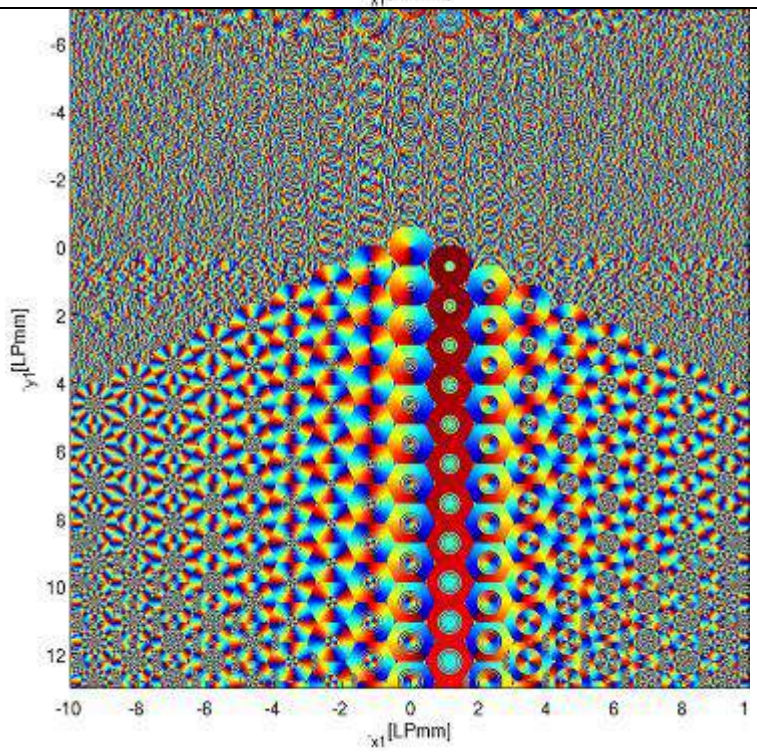

Gauss-Bessel Double Sum correlation

	Cor Four Int	Cor Four phase
ℓ / p	2	
-2	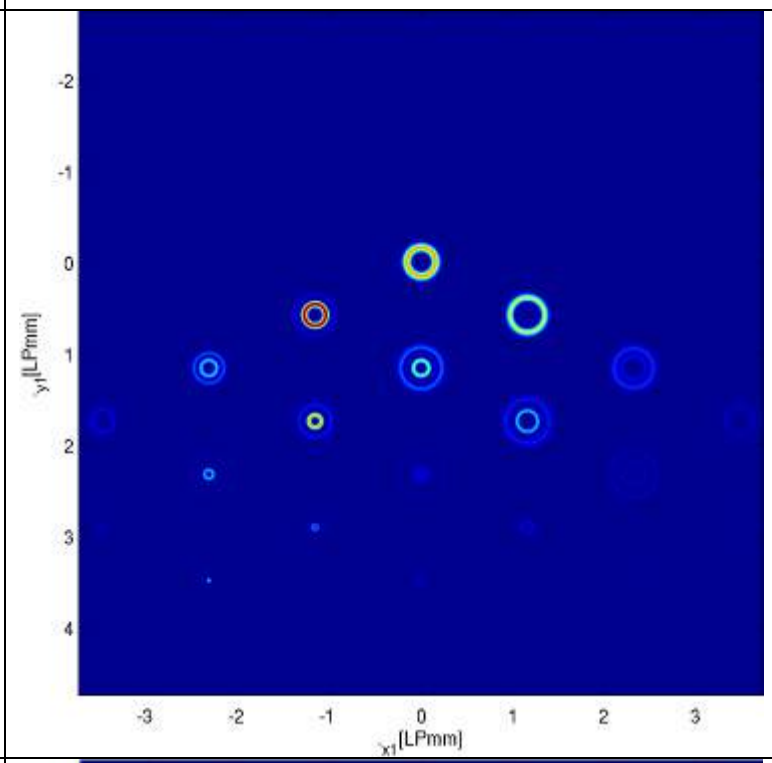	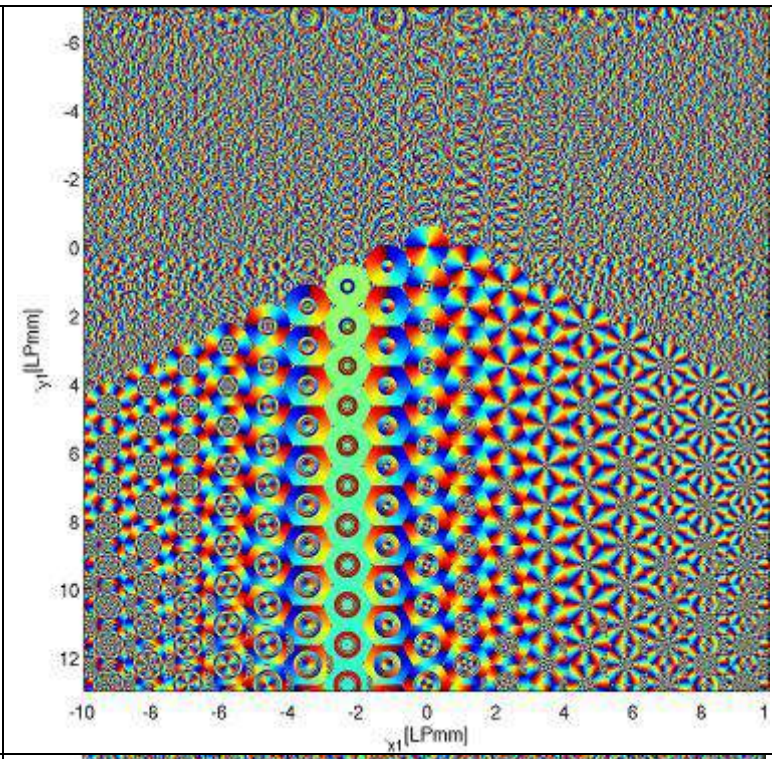
3	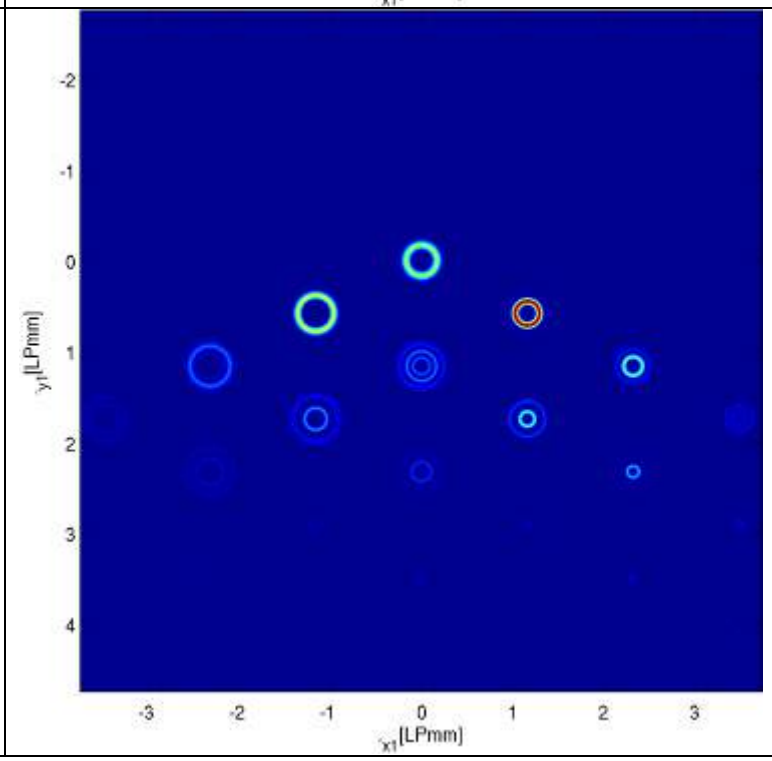	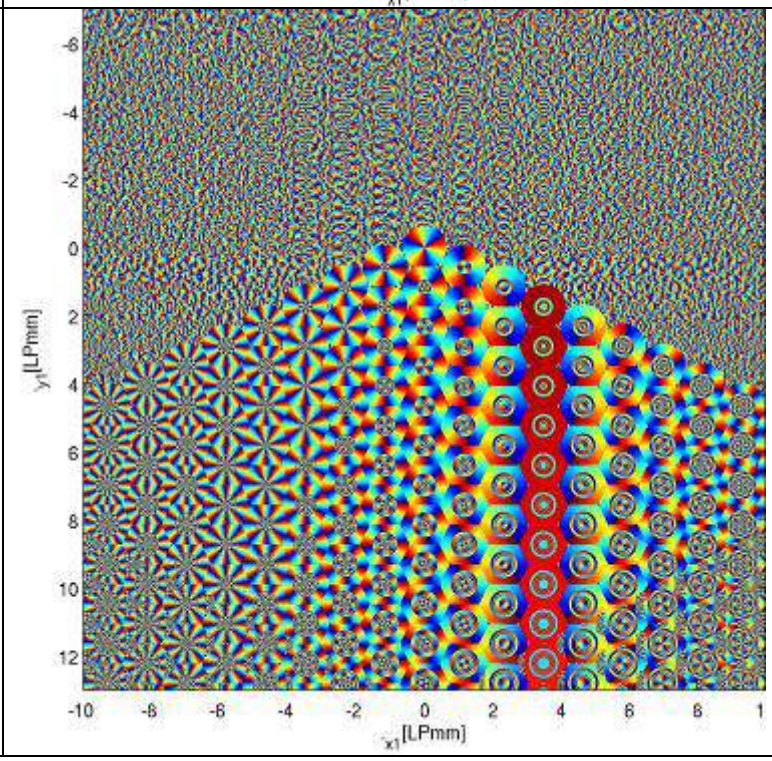

Gauss-Bessel Double Sum correlation

Gauss-Bessel Double Sum conclusions:

It seems the simulations for the Gauss-Bessel Double Sum formula agree greatly with the predictions made in chapter 3.

The Gauss-Bessel Double Sum LHS (left hand side) of eq.46 is good choice for an optical filter (correlator) for the purposes demultiplexing separate Gauss-Laguerre modes.

Summery and conclusions

This study's simulation results are in agreement with Shoam Shwartz study as it appears on the paper of [ii].
(S.Shwartz, M. A. Golub, and S. Ruschin," Diffractive optical elements for mode-division multiplexing of temporal signals with the aid of Laguerre–Gaussian modes" ,Appl. Opt .52, 2659-2669 (2013))

A method for improving this study results may be, using the *Rayleigh-Sommerfeld* model of Eq.7 instead of the *Fresnel Kirchhoff* approximation of Eq.19, as the former will predict the experiment with a greater degree of accuracy.

Also, it is preferable to redo the simulations that were carried out here again in a few years as stronger computing power will exist which will give better figures in images.

Finally, a great improvement (which is simple) will be to use an array of lenses to disable the parasitic parabolic phase, accumulated here due to using the far field approximation of Eq.20.

Reference

[i] N. Bozinovic, Y. Yue, Y. Ren, M. Tur, P. Kristensen, H. Huang, A. E. Willner, and S. Ramachandran, “Terabit-scale orbital angular momentum mode division multiplexing in fibers,” Science 340, 1545–1548 (2013).

[ii] S.Shwartz, M. A. Golub, and S. Ruschin,” Diffractive optical elements for mode-division multiplexing of temporal signals with the aid of Laguerre–Gaussian modes” ,Appl. Opt .52, 2659-2669 (2013).

[iii] R. Essiambre, "Overview of the Nonlinear Shannon Limit for Optical Fibers," in Latin America Optics and Photonics Conference, OSA Technical Digest (online) (Optical Society of America, 2012), paper LM1C.1

[iv] Gregory J. Gbur, Mathematical Methods for Optical Physics and Engineering, Cambridge, p.649

[v] Colton & Kress (1998) p. 32.
[vi] Cuyt *et al.* (2008) p. 344.
[vii] Szegö, G. Orthogonal Polynomials, 4th ed. Providence, RI: Amer. Math. Soc., 1975.
[viii] J.E. Wilhjelm, Bandwidth expressions of Gaussian Weighted Chirp, Electronics Letters, 09.12.93. Vol. 29. No. 25